A PRACTICAL, BASIC GUIDE TO

QUASI-GEOSTROPHIC THEORY

RESPONSE TO GEOSTROPHIC DEFORMATION

AGEOSTROPHIC MOTION

JET STREAKS

TED FUNK

Science and Operations Officer
National Weather Service
Louisville, Kentucky

February 2011

TABLE OF CONTENTS

QUASI-GEOSTROPHIC MOMENTUM EQUATIONS

Start with the ***TOTAL MOMENTUM EQUATIONS***:

1) $$\frac{du}{dt} = fv - g\frac{\partial z}{\partial x} - F_x$$

2) $$\frac{dv}{dt} = -fu - g\frac{\partial z}{\partial y} - F_y$$

Acceleration *Coriolis Force* *Pressure Gradient Force* *Friction*

Acceleration is a function of the Coriolis and pressure gradient forces, and friction.

u = east-west wind component
v = north-south wind component

The total derivative (du/dt) consists of a local change term ($\partial u/\partial t$) and horizontal ($u\,\partial u/\partial x + v\,\partial u/\partial y$) and vertical advection ($\omega \partial u/\partial p$) terms. Expanding 1) and 2) with advection terms on the right side yields:

3) $$\frac{\partial u}{\partial t} = -u\frac{\partial u}{\partial x} - v\frac{\partial u}{\partial y} - \omega\frac{\partial u}{\partial p} + fv - g\frac{\partial z}{\partial x} - F_x$$

4) $$\frac{\partial v}{\partial t} = -u\frac{\partial v}{\partial x} - v\frac{\partial v}{\partial y} - \omega\frac{\partial v}{\partial p} - fu - g\frac{\partial z}{\partial y} - F_y$$

The local change at a certain location (Eulerian approach) is being considered.

Assuming mid-latitude synoptic-scale flow (horizontal length scale ≥ 1000 km) above the boundary layer, a scale analysis indicates the vertical advection and friction terms are much smaller than the other terms and can be dropped. Also, the total wind consists of the geostrophic and ageostrophic wind, i.e., $u = u_g + u_{ag}$ and $v = v_g + v_{ag}$. Here, geostrophic motion is considered. Making these changes to Equations 3 and 4 results in the ***QUASI-GEOSTROPHIC MOMENTUM EQUATIONS***:

5) $$\frac{\partial u_g}{\partial t} = -u_g\frac{\partial u_g}{\partial x} - v_g\frac{\partial u_g}{\partial y} + fv - g\frac{\partial z}{\partial x}$$

6) $$\frac{\partial v_g}{\partial t} = -u_g\frac{\partial v_g}{\partial x} - v_g\frac{\partial v_g}{\partial y} - fu - g\frac{\partial z}{\partial y}$$

Local change in u_g and v_g *Horizontal advection of geo wind by the geo wind* *Coriolis Force* *Pressure Gradient Force*

MASS CONTINUITY EQUATION

This equation defines the relationship between horizontal and vertical divergence and convergence. In pressure coordinates, the ***MASS CONTINUITY EQUATION*** is:

7) $$\frac{\partial u_{ag}}{\partial x} + \frac{\partial v_{ag}}{\partial y} = -\frac{\partial \omega}{\partial p}$$

The equation states that **horizontal divergence (convergence) must equal vertical convergence (divergence)**. Notice that u and v (total wind components) are replaced by u_{ag} and v_{ag} (ageostrophic winds) since, by definition, the divergence of the geostrophic wind is zero. In other words, vertical motion (ω) is due to ageostrophic motion. Model vertical motion fields often reflect their own divergence/ convergence fields. **Figs. 1a and 1b** are two applications of the continuity equation.

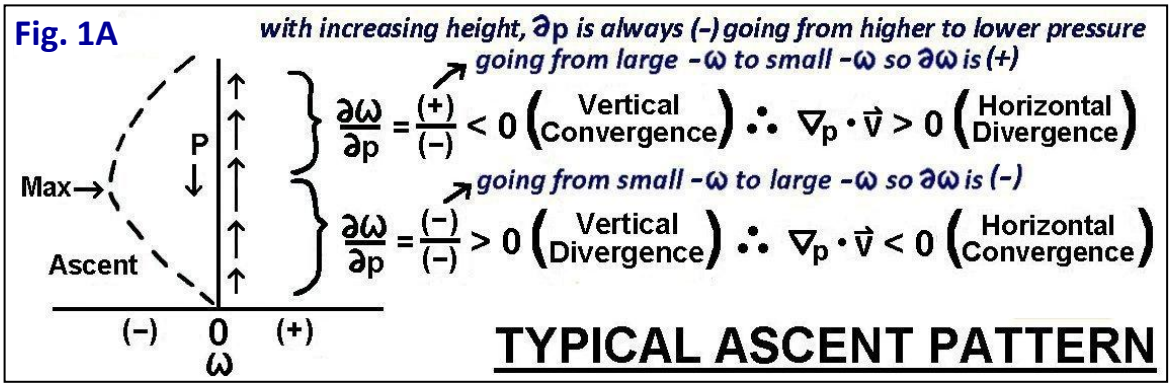

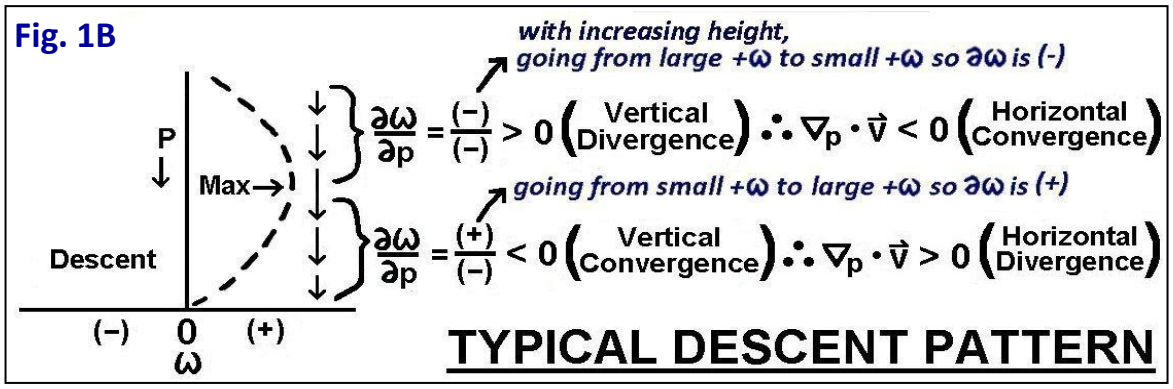

QUASI-GEOSTROPHIC VORTICITY EQUATION

The wind shear component of relative vorticity (ζ) is equal to $\partial v/\partial x - \partial u/\partial y$ (i.e., change in the north-south wind in the x direction [to the east] minus change in the east-west wind in the y direction [to the north]). If considering only QG relative vorticity, **ζ_g is related to the Laplacian of the height field**:

8) $$\zeta_g = \frac{g}{f_o}\nabla^2 z$$

where the horizontal Laplacian $\nabla^2 z = \partial^2 z/\partial x^2 + \partial^2 z/\partial y^2$. A Laplacian refers to the geometry or gradients of a parameter. If a parameter has a positive value, the Laplacian of the parameter generally is negative. Therefore, from Equation 8, the **geostrophic relative vorticity is inversely related to the height field, i.e., when z (height) is a maximum (minimum) in a ridge (trough) axis, then relative vorticity is a minimum (maximum)**. This makes sense! Using the local change of vorticity $(\partial\zeta_g/\partial t)$ and the quasi-geostrophic momentum and continuity equations, the ***QG VORTICITY EQUATION*** can be defined as:

9a) $$\frac{\partial \zeta_g}{\partial t} = \left[-\vec{V}_g \cdot \nabla(\zeta_g + f)\right] - f_o(\nabla \cdot \vec{V}) \qquad \text{or}$$

9b) $$\frac{\partial \zeta_g}{\partial t} = \left[-\vec{V}_g \cdot \nabla(\zeta_g + f)\right] + f_o(\partial\omega/\partial p)$$

Local change of geo relative vorticity — *Advection of absolute geo vorticity by geo wind* — *Horiz divergence (9a)/ vertical stretching (9b) term*

These equations state that **vorticity changes at a location are due to vorticity advection and horizontal convergence/vertical divergence. PVA (NVA) causes ζ_g to increase (decrease) with time. Horizontal**

convergence (divergence) results in vertical divergence (convergence) and thus a vorticity increase (decrease). It is easy to see how PVA and NVA affect vorticity at a point, but the equation's second term is also important. **Horizontal convergence causes vertical divergence which increases (spins-up) vorticity. This is very important, for example, on the scale of a thunderstorm updraft, i.e., vertical stretching occurs as the updraft velocity increases with height resulting in greater updraft rotation.**

QUASI-GEOSTROPHIC THERMODYNAMIC EQUATION

To determine how temperature is affected in the atmosphere and to derive the QG Omega Equation, from the First Law of Thermodynamics the ***QUASI-GEOSTROPHIC THERMODYNAMIC EQUATION*** is:

10) $$\frac{\partial T}{\partial t} = -\vec{V}_g \cdot \nabla_p T + \frac{P}{R}\sigma\omega + (Non\ QG\ Diabatic\ Effects)$$

Local change of temperature | *Horiz temp advection by the geo wind* | *Adiabatic heating/ cooling term* | *Diabatic effects (not QG)*

Equation 10 states that **quasi-geostrophic temperature change at a particular location and height is a function of temperature advection and vertical motion. Warm (cold) advection causes a temperature increase (decrease). Ascent ($\omega < 0$) causes adiabatic cooling and a temperature decrease ($\partial T/\partial t < 0$), while descent ($\omega > 0$) produces adiabatic heating**. These two terms often oppose each other. For example, strong warm advection at a level causes local warming, but often ascent as well. The ascent leads to adiabatic cooling opposing the warming due to warm advection. Given strong ascent, this can contribute to isotherms or thicknesses remaining steady or even sinking southward in the face of warm advection, which may be very important for heavy precipitation production. Models can show this process, which likely will be accompanied by areas of strong model upward motion. In borderline precipitation phase change situations, the absence of strong ascent can result in, for example, light rain or drizzle. However, if a burst of vertical motion (e.g., elevated slantwise or upright convection) develops in this area, strong adiabatic cooling can temporary cause a phase change to snow, with precipitation diminishing and changing back to liquid once the enhanced ascent zone moves away.

The **diabatic term** in Equation 10 **violates QG considerations**. However, **diabatic effects can have substantial effects on local atmospheric temperature.** For example, the melting of snow falling from a cold layer above into a warm layer below will cause cooling of the warm layer. Diurnal heating/cooling plays a major role in temperature changes near the surface. Also, strong ascent can result in significant **latent heat release** due to condensation of moisture. This **warming will oppose the adiabatic cooling due to lift, but net cooling should still occur due to ascent (the less moisture, the more the net cooling)**.

Finally, Equation 10 contains a static stability term (σ), proportional to $-\partial\theta/\partial p$. **When stability is large (tight vertical packing of potential temperature so $-\partial\theta/\partial p \gg 0$), adiabatic cooling due to lift will have a greater effect on temperature than for a relatively unstable atmosphere (little vertical packing of θ).**

As a sidelight, the ***HYDROSTATIC EQUATION*** is given by:

11) $$\frac{\partial z}{\partial p} = -\frac{RT}{pg}\ \ thus\ T = -\frac{pg}{R}\frac{\partial z}{\partial p} = -\frac{p}{R}\frac{\partial \Phi}{\partial p}$$

where geopotential height $\Phi = gz$. This equation states that the **vertical pressure gradient force** (upward force) **is balanced by gravity** (downward force). It also reveals that the **mean temperature in a layer is directly proportional to the thickness ($\partial z/\partial p$) of the layer.**

QUASI-GEOSTROPHIC HEIGHT TENDENCY EQUATION

The quasi-geostrophic vorticity, thermodynamic, and mass continuity equations can be combined to determine where highs and lows (ridges and troughs) are moving, i.e., what the height changes will be. This is addressed through the ***QUASI-GEOSTROPHIC HEIGHT TENDENCY EQUATION***:

12) $$\left[\nabla_p{}^2 + \frac{f_o{}^2}{\sigma}\frac{\partial^2}{\partial p^2}\right]\chi = f_o\left[-\vec{V}_g \cdot \nabla_p(\zeta_g + f)\right] - \frac{f_o{}^2}{\sigma}\frac{\partial}{\partial p}\left[\frac{R}{P}\left(-\vec{V}_g \cdot \nabla_p T\right)\right]$$

Laplacian of height tendency, $\chi = \partial\Phi/\partial t$ *Vorticity advection* *Differential temperature advection*

***Vorticity advection term*:**

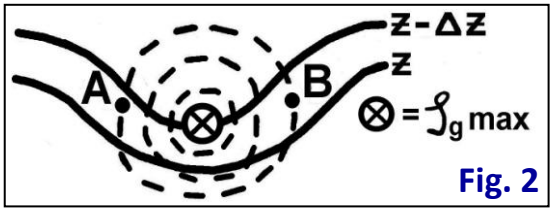

Fig. 2

For PVA (occurring at Point B in **Fig. 2**), this term is > 0, so on the left side of Equation 12, $\nabla^2\chi > 0$, so $\chi < 0$ (height falls). Thus, **PVA at a level causes height falls**. For NVA (Point A), this term is < 0, so $\nabla^2\chi < 0$, so $\chi > 0$ (height rises). Thus, **NVA at a level causes height rises**. Another way to look at this is to consider Equation 8 which relates geostrophic vorticity to the Laplacian of the height field. **If PVA (NVA) is occurring at a certain location, then vorticity (ζ_g) is increasing (decreasing), and from Equation 8, $\nabla^2 z$ must be increasing (decreasing) so "z" (height) must be decreasing/height falls (increasing/height rises).**

***Differential temperature advection term*:**

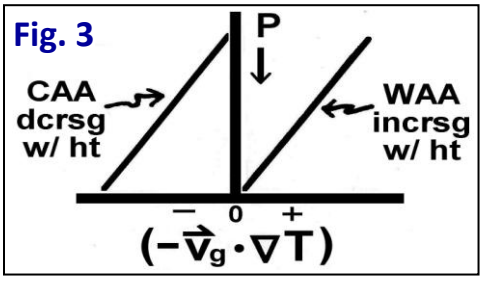

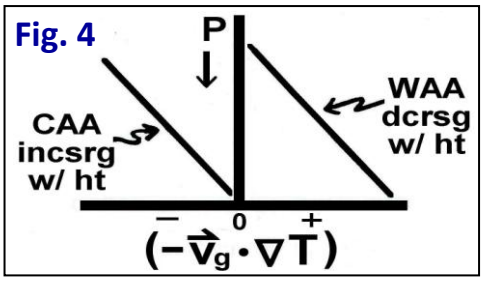

Temperature advection (TA) at multiple levels must be considered. **Fig. 3** shows cold air advection (CAA) decreasing with height (increasing with pressure) and warm advection (WAA) increasing with height (decreasing with pressure), which have the same effect. From Equation 12, this means $\partial/\partial p[TA] < 0$ causing $\nabla^2\chi > 0$, so $\chi < 0$ (height falls). In **Fig. 4**, the opposite is occurring. CAA is increasing with height (decreasing with pressure) and WAA is decreasing with height (increasing with pressure). This causes $\partial/\partial p[TA] > 0$, so $\nabla^2\chi < 0$, so $\chi > 0$ (height rises).

In general, **temperature advection increasing (decreasing) with height causes height falls (rises). Cold advection below a 500 mb trough deepens the trough, while warm advection below a 500 mb ridge builds the ridge. Therefore, differential temperature advection intensifies upper troughs and ridges in developing synoptic waves.**

Considering the effect of temperature advection (TA) on heights and thickness in another way, **Fig. 5** assumes WAA at all levels, but is a maximum at 800 mb. TA increasing with height below 800 mb causes height falls, while TA decreasing with height above 800 mb causes height rises. The effect of this

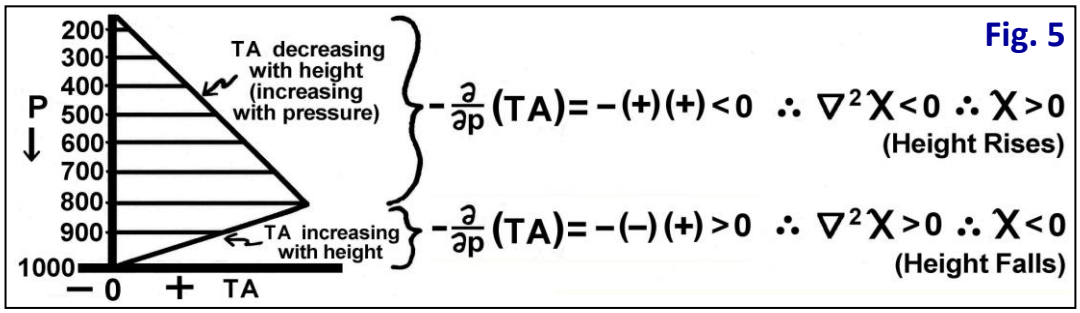

advection pattern on thickness is shown in **Fig. 6**. The solid (dashed) lines are old (new) pressure surfaces before (after) the warm air advection (WAA) pattern in **Fig. 5**. Above 800 mb, the WAA pattern causes height rises (**Fig. 5**) which "push" pressure surfaces upward (**Fig. 6**). Below 800 mb, it causes height falls (**Fig. 5**) which "push" pressure surfaces downward (**Fig. 6**). At the level of maximum WAA at 800 mb, there is no height change. What results from this typical temperature advection pattern is that 1000-500 mb layer thickness (from below to above the maximum WAA at 800 mb) increases.

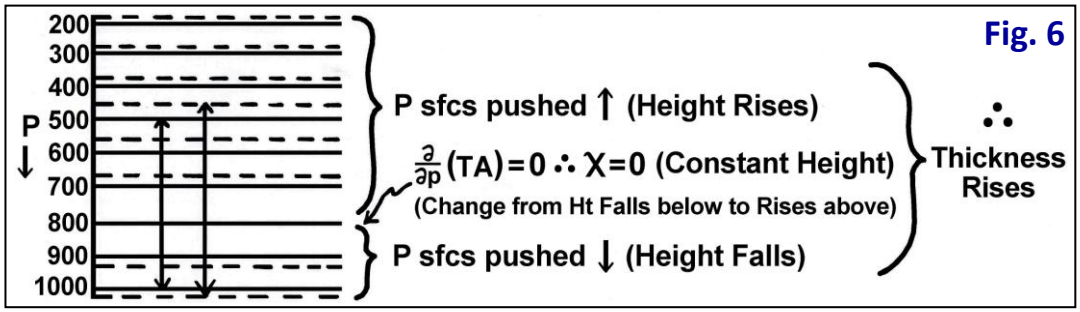

Overall, **warm (cold) air advection causes height rises above (below) the level of maximum advection and height falls below (above) the maximum, resulting in an increase (decrease) in layer thickness.**

QUASI-GEOSTROPHIC OMEGA EQUATION

The quasi-geostrophic vorticity, thermodynamic, and continuity equations can be combined to determine the distribution of synoptic-scale vertical motion through the ***QUASI-GEOSTROPHIC OMEGA EQUATION***:

$$13)\quad \left[\nabla_p^{\,2} + \frac{f_o^{\,2}}{\sigma}\frac{\partial^2}{\partial p^2}\right]\omega = -\frac{f_o}{\sigma}\frac{\partial}{\partial p}\left[-\vec{V}_g \cdot \nabla_p(\zeta_g + f)\right] - \frac{R}{\sigma p}\nabla_p^{\,2}\left[-\vec{V}_g \cdot \nabla_p T\right]$$

Laplacian of vertical motion (ω) — *Differential vorticity advection* — *Laplacian of temperature advection*

The main difference between this and the Height Tendency Equation (12) is that Equation 12 is integrated with respect to pressure ($\partial/\partial p$) to determine ω in Equation 13. Only derivatives in space (not time) are in 13. Thus, it is a diagnostic measure of vertical motion (ω) based on geopotential height. Consider each term's effect on ω.

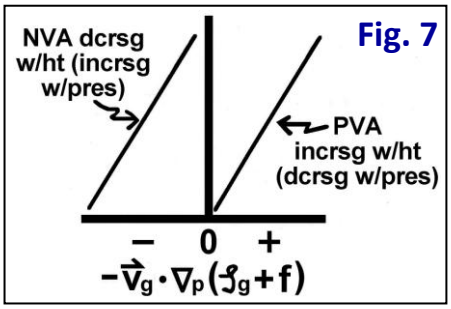

***Differential vorticity advection term*:**

Fig. 7 shows a profile of PVA increasing with height (decreasing with pressure) and NVA decreasing with height (increasing with pressure), which have the same effect. This causes $\partial/\partial p[VA] < 0$, so $\nabla^2\omega > 0$

(negative sign in front of this term), so $\omega < 0$ (upward motion). Similarly, PVA decreasing with height and NVA increasing with height causes $\omega > 0$ (downward motion).

Overall, **vorticity advection (VA) increasing with height forces synoptic-scale upward motion. Equation 13 states that VA at 500 mb alone DOES NOT force vertical motion; the change of VA with height does.** For example, there could be no PVA or even NVA at 500 mb but PVA above 500 mb. This increasing PVA with height would be forcing for synoptic-scale ascent despite the 500 mb pattern.

Mathematically, it makes sense how differential vorticity advection causes vertical motion, but how this occurs physically is shown in **Fig. 8**. Assume a profile of PVA increasing with height (**Fig. 8A**). At height level $h1$, there is weak PVA while at the higher level $h2$ there is stronger PVA. Thus, relative vorticity (ζ_g) is increasing some at $h1$ but more so at $h2$. From Equation 8 which relates vorticity to the Laplacian of heights (z), at $h1$ a small height fall occurs (i.e., since $\zeta_g > 0$, then $\nabla^2 z > 0$, so $z < 0$), while at $h2$ the larger vorticity increase results in a larger height fall than at $h1$ (**Fig. 8B**).

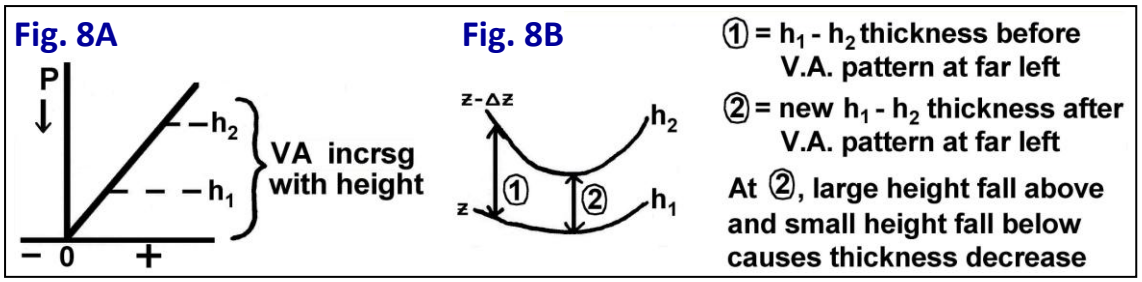

The net result of small height falls below and larger falls above is that the thickness of the "$h1 - h2$" layer decreases. In other words, **a thickness decrease will occur in a layer in which VA increases with height**. As a result, **to keep the atmosphere hydrostatic, this thickness decrease must be accompanied by a decrease in the mean temperature of the layer**. Using the QG thermodynamic equation (Equation 10), $\partial T/\partial t$ must be < 0. **To do this, ascent ($\omega < 0$) must occur so that the adiabatic term in Equation 10 results in adiabatic cooling**. Similarly, **VA decreasing with height results in a thickness increase, which must be accompanied by adiabatic warming through descent ($\omega > 0$)**. This QG discussion explains how differential VA leads to vertical motion. Differential VA does not ***cause*** vertical motion; it ***forces*** it through atmospheric response.

***Laplacian of temperature advection term*:**

This term relates temperature advection (TA) to vertical motion. If **warm air advection** is occurring, then $TA > 0$, so $\nabla^2(TA) < 0$, but the negative sign in front of this term makes $\nabla^2\omega > 0$, so $\omega < 0$ (**upward motion**). Similarly, **cold advection** leads to $\omega > 0$ (**downward motion**). However, technically TA alone does not define the vertical motion field. The geometry or gradients (Laplacian) of TA must be considered. **Vertical motion (ω) is greatest when the gradients of TA are large**. The Laplacian of a parameter is greatest when a circular pattern exists with a parameter maximum in the center and a strong gradient surrounding the maximum (i.e., "bullseye" pattern). Therefore, although TA itself is normally associated with vertical motion, it is best to **consider *the pattern* of TA, i.e., QG upward motion likely is greatest where concentric maxima (bullseyes) of WAA exist**.

Mathematically, temperature advection leads to vertical motion. But, to determine how this occurs physically and why WAA forces upward motion, consider **Fig. 9**.

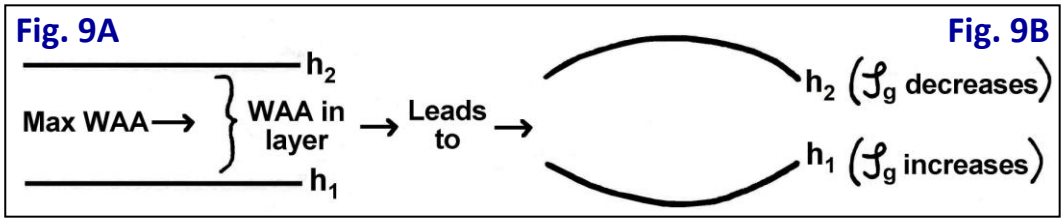

Before WAA begins (**Fig. 9A**), $h1$ and $h2$ are lower and upper height levels. Once WAA occurs in this layer, from the differential temperature advection term in Equation 12 **heights rise (fall) above (below) the level of maximum WAA** (between $h1$and $h2$). **This causes a *relative* increase in vorticity (trough) at the bottom and a *relative* decrease in vorticity (ridge) at the top of the layer** (**Fig. 9B**). Ignoring the vorticity advection term in the QG Vorticity Equation (Equations 9a/9b), at the bottom of the layer ($h1$), $\partial\zeta_g/\partial t > 0$ which means convergence must occur. At the top ($h2$), $\partial\zeta_g/\partial t < 0$, requiring divergence. Thus, **WAA has resulted in low-level convergence and upper-level divergence. The Continuity Equation (7) states that upward motion must occur given this profile**. Similarly, CAA generally leads to relative convergence aloft and divergence below, and subsequent downward motion.

Differential vorticity advection and the Laplacian of temperature advection are **forcing mechanisms** for synoptic-scale vertical motion (Equation 13). The left side of the QG omega equation is a Laplacian of vertical motion (ω). Within this Laplacian, there is a **static stability parameter (σ), which is important.** In general, **the lower (higher) the static stability, i.e., the more unstable (stable) it is, the greater (less) will be the vertical motion response to forcing. In other words, the same amount of forcing in a relative unstable (stable) atmosphere generally will cause stronger (weaker) vertical motion.**

The **two forcing terms in the QG Omega Equation oppose each other in certain areas**. Examples are just downstream from a trough axis aloft where mid-to-upper-level differential PVA and low-to-mid-level CAA may be coincident, and near the top of a ridge axis where low-to-mid-level WAA and mid-to-upper-level neutral or even NVA may be occurring. An example is shown in **Fig. 10**. The circled area is experiencing assumed differential PVA (**Fig. 10A**), but also low-level CAA (**Fig. 10B**). Thus, it can be difficult to determine which forcing term is more important and what type of vertical motion is occurring. These problems have been addressed by alternative approaches to the traditional QG Omega Equation, including the Trenberth (1978) and Q-Vector methods which are discussed below.

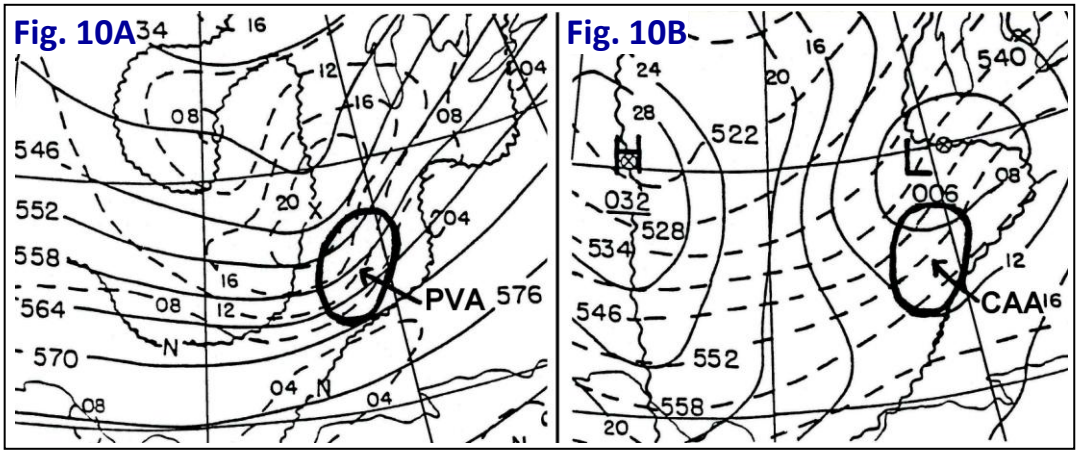

An idealized QG description of a mid-latitude baroclinic wave with respect to vorticity, height tendency, thickness, and vertical motion is summarized in **Fig. 11**. A graphical summary of the relationships between temperature advection patterns and the response of height, divergence, vorticity, and vertical motion is presented in **Figs. 12A and 12B**.

Fig. 11

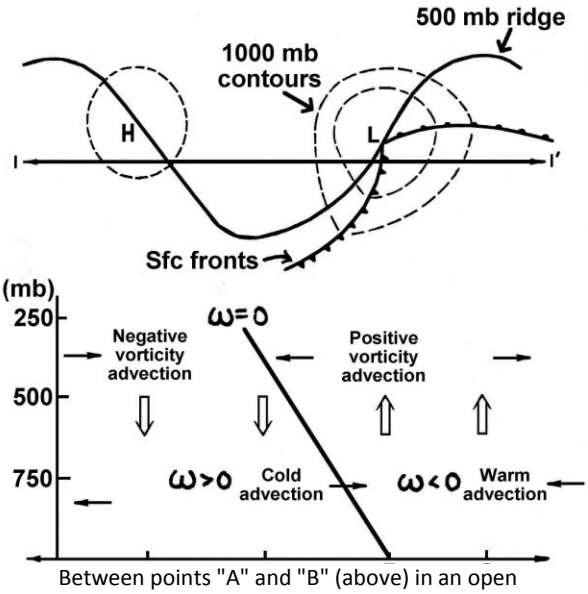

Between points "A" and "B" (above) in an open synoptic wave, CAA is occurring in lower levels with PVA in upper levels. Thus, what is the atmospheric vertical motion response in this area?

Idealized QG Description of a Mid-Latitude Baroclinic Wave

Parameter	A: 500 mb trough	B: Sfc low	C: 500 mb ridge	D: Sfc high
ζ_g at 500 from QG Vorticity Eq.	Increasing due to convergence* (no VA)	Increasing due to PVA; partly cancelled by divergence	Decreasing due to divergence* (no VA)	Decreasing due to NVA; partly cancelled by convergence
ω at 500 from QG Omega Eq.	Sinking due to CAA (no VA)	Rising due to differential PVA (TA small)	Rising due to WAA (no TA)	Sinking due to differential NVA (TA small)
Ht. Tendency (χ) at 500 mb from Ht. Tendency Eq.	Decreasing due to TA increasing with height	Decreasing due to PVA	Increasing due to TA decreasing with height	Increasing due to NVA
Thickness from 1000-500 mb	Decreasing due to CAA; partly cancelled by adiabatic warming	Decreasing due to adiabatic cooling (TA small)	Increasing due to WAA; partly cancelled by adiabatic cooling	Increasing due to adiabatic warming (TA small)
ζ_g at sfc from QG Vorticity Eq.	Decreasing due to divergence (VA small)	Increasing due to convergence (VA small)	Increasing due to convergence (VA small)	Decreasing due to divergence (VA small)

*Assumes level of non-divergence is below 500 mb

LEGEND: VA : Vorticity Advection; TA : Temperature Advection; PVA : Positive Vorticity Advection; NVA : Negative Vorticity Advection; CAA : Cold Air Advection; WAA : Warm Air Advection

Relationship Between Temp Advection & Response of Height, Omega, Divergence, and Vorticity

Vertical Profile of Temperature Advection	Temperature Change	QG Height Change	QG Vertical Motion (ω)	Divergence Response (Vert CON/DIV requires Horiz DIV/CON)	Vorticity Response $\frac{\partial \zeta_g}{\partial t} \propto -DIV$
P ↓ 200 / 500 / 1000; CAA(-) 0 WAA(+)	Warming (dcrsg w/ht) Max Warming Warming (incrsg w/ht)	Rise Fall	$\omega<0$ $\omega<0$ (max) $\omega<0$	DIV None CON	$\frac{\partial \zeta_g}{\partial t}<0$ $\frac{\partial \zeta_g}{\partial t}=0$ $\frac{\partial \zeta_g}{\partial t}>0$
P ↓ 200 / 500 / 1000; CAA(-) 0 WAA(+)	Warming (incrsg w/ht) No Change Cooling (dcrsg w/ht)	Fall Fall	$\omega<0$ $\omega=0$ $\omega>0$	CON CON CON	$\frac{\partial \zeta_g}{\partial t}>0$
P ↓ 200 / 500 / 1000; CAA(-) 0 WAA(+)	Max Warming (T.A. incrsg w/ht) Small Warming	Fall Fall	$\omega<0$ (max) $\omega<0$ (min)	CON CON	$\frac{\partial \zeta_g}{\partial t}>0$ $\frac{\partial \zeta_g}{\partial t}>0$

Fig. 12A

Relationship Between Temp Advection & Response of Height, Omega, Divergence, and Vorticity

Vertical Profile of Temperature Advection	Temperature Change	QG Height Change	QG Vertical Motion (ω)	Divergence Response (Vert CON/DIV requires Horiz DIV/CON)	Vorticity Response $\frac{\partial f_g}{\partial t} \propto -DIV$
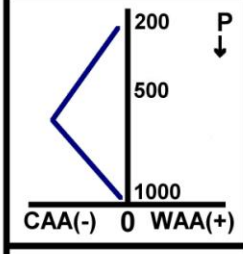	Cooling (dcrsg w/ht) Max Cooling Cooling (incrsg w/ht)	Fall Rise	ω>0 ω>0 (max) ω>0	CON None DIV	$\frac{\partial f_g}{\partial t}>0$ $\frac{\partial f_g}{\partial t}=0$ $\frac{\partial f_g}{\partial t}<0$
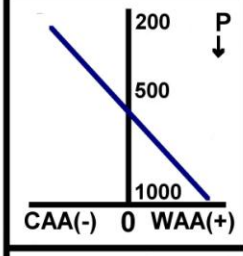	Cooling (incrsg w/ht) No Change Warming (dcrsg w/ht)	Rise Rise	ω>0 ω=0 ω<0	DIV DIV DIV	$\frac{\partial f_g}{\partial t}<0$
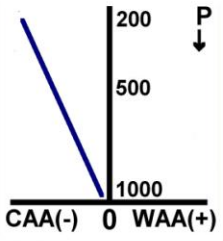	Max Cooling (T.A. dcrsg w/ht) Small Cooling	Rise Rise	ω>0 (max) ω>0 (min)	DIV DIV	$\frac{\partial f_g}{\partial t}<0$ $\frac{\partial f_g}{\partial t}<0$

Fig. 12B

ALTERNATIVE QG OMEGA EQUATION APPROACH: TRENBERTH METHOD

The vorticity and thermal advection terms of the traditional QG Omega Equation (13) often at least partially cancel each other out in some locations, leaving in doubt the sign of vertical motion. **Fig. 10** illustrated this point. Therefore, alternative forms of the traditional equation were formulated. For example, Trenberth (1978) modified the right side of Equation 13 to come up with the ***TRENBERTH QG OMEGA EQUATION***:

14) $$\left[\nabla_p{}^2 + \frac{f_o{}^2}{\sigma}\frac{\partial^2}{\partial p^2}\right]\omega = \frac{2f_o}{\sigma}\frac{\partial \vec{V}_g}{\partial p}\cdot\nabla_p\zeta_g$$

Laplacian of vertical motion (ω)

Advection of geostrophic vorticity by the vertical change of the geostrophic wind

The right side of this equation is **not** equivalent to the right side of the traditional QG Omega Equation (13). Equation 14 neglects a "deformation term," which is small near 500 mb but could be large near upper-level fronts and jets. Thus, the Trenberth method is more approximate than the traditional method, especially near jets, although it is simpler since the Trenberth scheme contains only one forcing

term. On the right side of Equation 14, $\partial\vec{V}_g/\partial p$ is the change of the geostrophic wind with pressure and can be written as $\Delta\vec{V}_g/\Delta p$. The thermal wind ($\vec{V}_T$) is defined as the vector difference between the geostrophic wind at two levels, i.e., $\vec{V}_T = \Delta\vec{V}_g = \vec{V}_{g\,(upper)} - \vec{V}_{g\,(lower)}$ so the term $\partial\vec{V}_g/\partial p$ is proportional to the thermal wind. Therefore, Equation 14, in effect, states that vertical motion (ω) is forced by the advection of geostrophic vorticity by the thermal wind. Since **the thermal wind is parallel to thickness lines** (whereby curvature and shear of thickness lines represent "thermal vorticity"), **forcing for QG vertical motion can be evaluated in observations and models by overlaying thickness (e.g., 700-300 mb) (not height) with vorticity (e.g., 500 mb), then determining areas of PIVA (Positive Isothermal Vorticity Advection) or TAV (Thermal Advection of Vorticity).** The PIVA Trenberth method is a quick, easy way to estimate large-scale vertical motion from synoptic charts, which approximately simulates the combined effect of differential vorticity advection and the Laplacian of temperature advection from Equation 13.

ALTERNATIVE QG OMEGA EQUATION APPROACH: Q VECTOR METHOD

Hoskins et al. (1978, 1980) derived another simpler approach to the traditional QG Omega Equation which does not neglect any terms as does the Trenberth method. A derivation results in the ***Q VECTOR QG OMEGA EQUATION***:

15) $$\left[\nabla_p{}^2 + \frac{f_o{}^2}{\sigma}\frac{\partial^2}{\partial p^2}\right]\omega = -2\nabla_p \cdot \vec{Q}$$

In this equation, $\vec{Q}$ is given by Equation 16.

16) $$\vec{Q} = -\frac{R}{\sigma p}\begin{bmatrix}\frac{\partial v_g}{\partial x}\cdot\nabla_p T \\ \frac{\partial v_g}{\partial y}\cdot\nabla_p T\end{bmatrix} = \begin{matrix} Q_1 = -\frac{R}{\sigma p}\left[\frac{\partial u_g}{\partial x}\frac{\partial T}{\partial x} + \frac{\partial v_g}{\partial x}\frac{\partial T}{\partial y}\right] = Q_x\,(W-E\ direction) \\ Q_2 = -\frac{R}{\sigma p}\left[\frac{\partial u_g}{\partial y}\frac{\partial T}{\partial x} + \frac{\partial v_g}{\partial y}\frac{\partial T}{\partial y}\right] = Q_y\,(N-S\ direction)\end{matrix}$$

Q vectors are not physical entities; they do not exist. They arise mathematically and represent a simple way to express their actual definition on the right side of Equation 16. They help to explain the results of physical processes in the atmosphere, and are useful diagnostic tools. **Q vectors represent the advection of the temperature gradient by the horizontal change in the geostrophic wind**. **Q vectors also can be defined as the vector rate of change of the temperature gradient** following an isobaric trajectory. **Their magnitude is proportional to the rate of horizontal change of the geostrophic wind at a particular level and the strength of the horizontal temperature gradient.**

Q vectors can be plotted at specific atmospheric levels or layers, and **contain both terms of the traditional QG Omega Equation. Divergence fields of Q vectors represent forcing for synoptic-scale vertical motion**. If there is convergence of Q, then $\nabla \cdot Q < 0$ (definition of convergence), so $-\nabla \cdot Q > 0$, so $\nabla^2\omega > 0$ meaning $\omega < 0$ (ascent). **In general, convergence (divergence) of Q vectors represents synoptic-scale forcing for upward (downward) motion. In all forms of the QG Omega Equation, the terms on the right side are forcing mechanisms which act to disrupt geostrophic balance. Vertical motion (ω) is the actual response to this forcing which attempts to restore geostrophic and thermal wind balance. These are large-scale motions, and do not account for mesoscale and convective-scale ascent/descent, which can be much greater and overwhelm QG vertical motions**.

There are several advantages to using Q vectors:

1) There is no vertical derivative. Therefore, Q vectors can be evaluated on individual pressure surfaces, in mean layers (e.g., 850-700 mb, 700-500 mb), and in spatial-height cross-sections in AWIPS. This allows for visualization of the depth and steepness of Q divergence/convergence (forcing) fields.

2) There is no "two-term conflict" as in the traditional form of the QG Omega Equation.

3) The equation does not neglect any terms, such as deformation in the Trenberth method. However, the QG system neglects advections by and temporal changes in the ageostrophic wind, friction, diabatic effects, and the vertical advection of ω, all which can be significant at times.

4) **Q vectors are closely related to ageostrophic flow. The magnitude of a Q vector is roughly proportional to the strength of the ageostrophic horizontal wind. Q vectors are pointed in the same direction as horizontal ageostrophic winds below the level Q is being looked at (i.e., same direction as the lower-branch of an ageostrophic circulation), and in the opposite direction above this level.**

5) **Q vectors are closely related to geostrophic frontogenesis. Where Q vectors point across isotherms/ thicknesses from cold to warm (warm to cold) air, frontogeneis or intensification of the thermal gradient (frontolysis or dissipation of the thermal gradient) is implied. Where frontogenesis is indicated, baroclinicity, wind convergence, and resultant ascent are increasing, with available potential energy being converted to kinetic energy. Frontogenesis may result in a band(s) of heavier precipitation roughly parallel to a frontal zone within a larger precipitation shield.**

Some illustrations of Q vectors and frontogenesis follow.

Fig. 13 depicts the effect of Q vector "cross-isotherm flow" on frontogenesis. Dashed lines are isotherms; arrows are Q vectors. Assume an initial homogeneous temperature gradient (**Fig. 13A**) with Q vectors pointing in the directions indicated. The area where Q vectors point from cold to warm air is frontogenetic with a tightening of the thermal gradient (**Fig. 13B**), creating an ascent response and precipitation assuming adequate moisture. The "flow" from warm to cold air suggests frontolysis and a weakening of the thermal gradient and vertical motion field. Model mass fields continually respond to and readjust the atmosphere based on their own frontogenetical forcing.

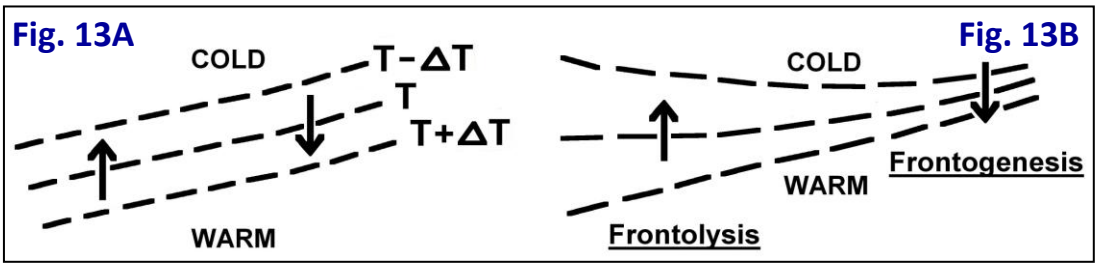

An example from AWIPS (**Fig. 14**) shows data in the 850-700 mb layer from the GFS model at 00 UTC 23 December 2004. The storm brought intense snowfall (up to 30 inches) and thunder to southern Indiana and heavy sleet to north-central Kentucky. Saturation (pink color in relative humidity image) was present over the Lower Ohio and Tennessee Valleys. A strong thermal gradient (green isotherms) existed from Ohio to the Lower Mississippi Valley (**Fig. 14A**). Q vectors (yellow arrows) were directed from cold to warm air in this axis, where broad QG frontogenesis existed (solid blue lines in **Fig. 14B**). **Q vector length is directly proportional to the amount of QG frontogenesis**. This provided synoptic forcing for lift in the

area of moisture. Conversely, from eastern Kansas to northeastern Texas, Q vectors pointed from warmer to colder air (**Fig. 14A**), indicative of QG frontolysis (dashed lines in **Fig. 14B**).

Fig. 14A

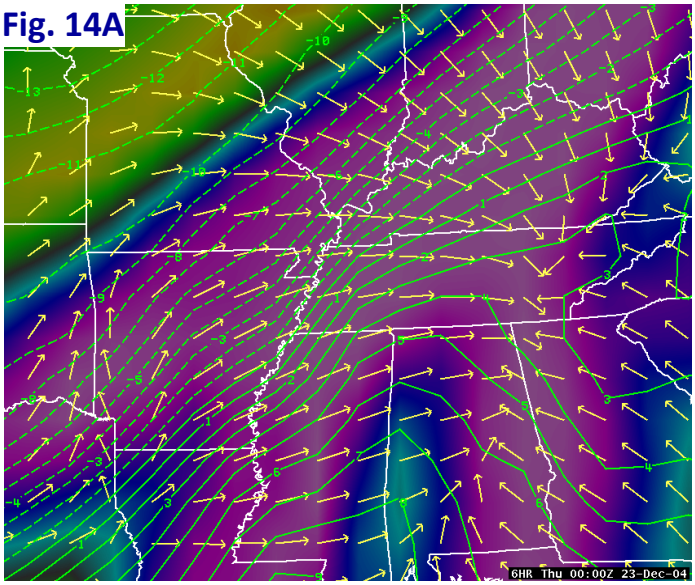

Fig. 14B

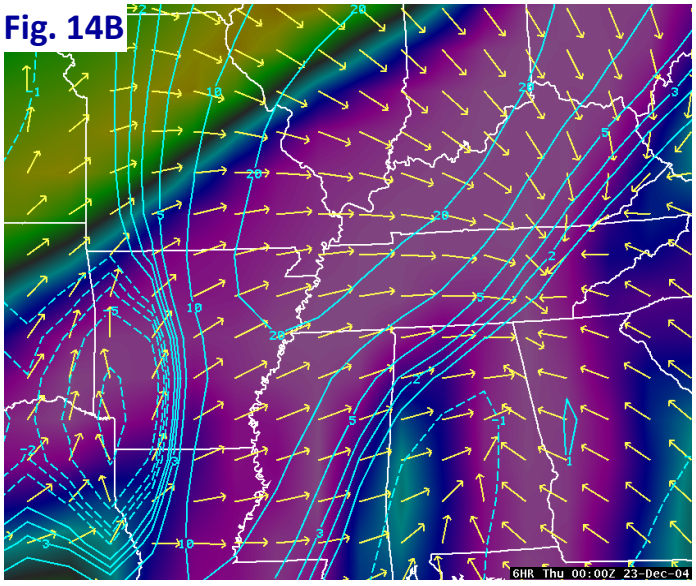

Derived from **Fig. 14B**, **Fig. 14C** portrays 850-700 mb layer Q vectors and Q vector divergence at 00 UTC 23 December. Dashed lines show convergence or forcing for synoptic scale ascent, with a maximum from southern Indiana to Alabama. Q vector divergence (forcing for synoptic descent) is noted from southern Missouri to Louisiana.

Fig. 14C

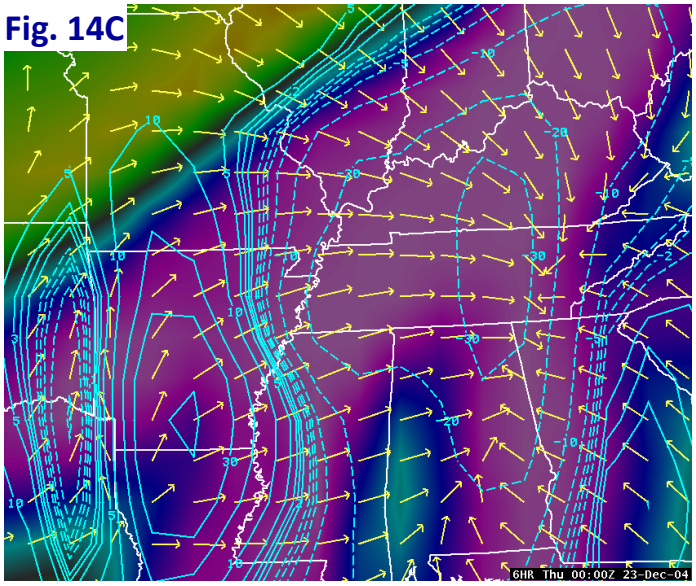

Fig. 15A shows frontogenesis ("F") vectors and two-dimensional frontogenesis (Petterssen 1956), while **Fig. 15B** depicts F vector divergence for the same layer and time period as in **Fig. 14**. **Fig. 15A** is analogous to **Fig. 14B**, except the actual wind (geostrophic and ageostrophic components) is used to compute F vectors and frontogenesis in **15A**, while QG frontogenesis in **14B** is based on the geostrophic wind only. Similarly, **Fig. 15B** is the full wind version of the QG analysis in **Fig. 14C**, where dashed (solid) contours represent convergence (divergence) of F vectors. In general, **the axis of F/Q vector convergence normally is located just to the right (south or east side) of the maximum frontogenetical axis.** Q vector convergence represents forcing for ascent via the Q vector version of the QG Omega Equation (15); F vector convergence technically does not since it is based on the total wind. Nevertheless, areas of F vector convergence often are associated with zones of enhanced frontal scale or mesoscale lift due to the direct thermal ageostrophic circulation forced by the 2-D frontogenesis, which in turn can lead to banded precipitation structure. This is particularly true in a deepening, baroclinic system.

The location of the responsive ascent normally is within the axis of maximum F/Q vector convergence at the particular level or layer being diagnosed. However, since baroclinic systems slope with height toward cold air, the **frontogenetical surface usually slopes with height toward cold air** as well. Thus, depending on the vertical slope and depth of the frontogenetical forcing and associated isentropes, as well as the amount of moisture and ambient atmospheric stability, the **heaviest precipitation often falls** just outside

Fig. 15A

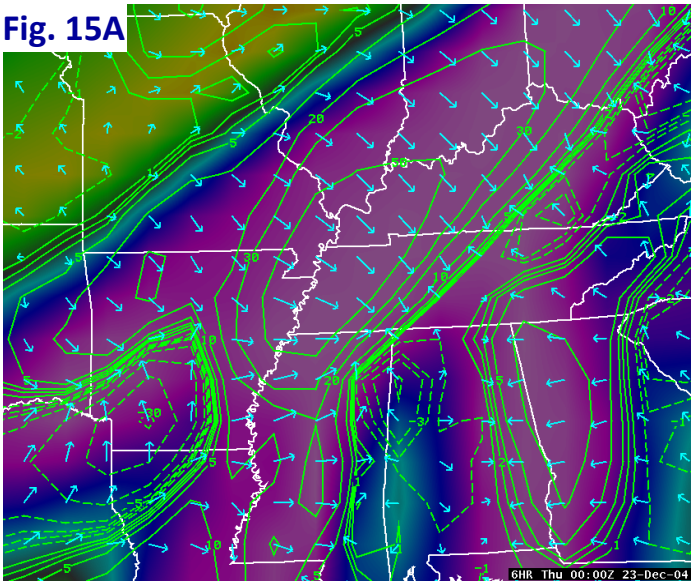

Fig. 15B

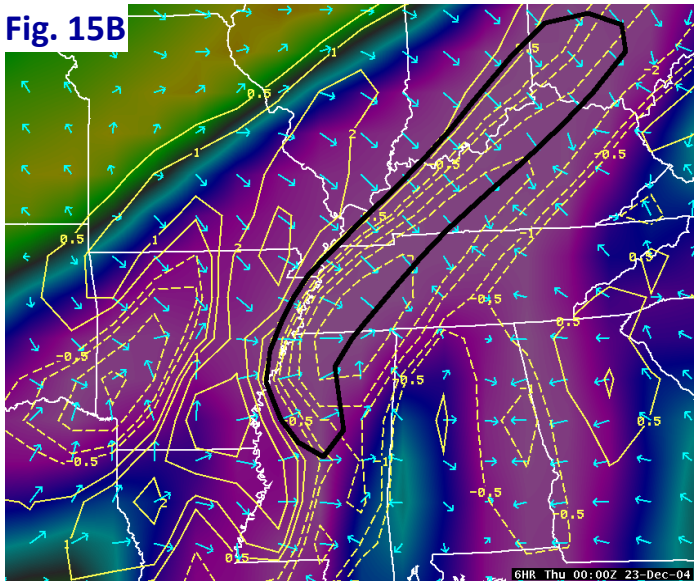

the axis of maximum low-level (850 mb) forcing. Instead, it occurs roughly **along the center line of the axis of maximum 850-700 mb layer F vector convergence back through the gradient zone between the layer F vector convergence and F vector divergence just to the north or west** (area inside the black line in **Fig. 15B**). Precipitation can also occur within the 850-700 mb F vector divergence area, especially for a gradually sloped system with height. The stronger and tighter the F/Q vector convergence/divergence couplets (e.g., in **Fig. 15B**), the greater the potential for significant vertical motion, particularly if the atmosphere is only marginal stable or unstable to slantwise or upright convection.

F (Q) vectors can be broken into two components, i.e., F_n and F_s (Q_n and Q_s) vectors (natural coordinates) (**Fig. 16**). F_n (Q_n) is the **frontogenetical component** of F (Q), and is directed perpendicular to isotherms/thicknesses. F_s (Q_s) is the **rotational component** of F (Q), and is directed parallel to isotherms. F_n often is the dominant term and forces vertical motion on the mesoscale/frontal scale. It describes how the magnitude of the thermal gradient is changing, i.e., whether it is strengthening (frontogenesis) via confluence or weakening (frontolysis) via difluence. F_s describes temperature advection patterns, and forces vertical motion on the synoptic scale. It describes how the orientation of isotherms/thicknesses is changing with time due to horizontal changes in the wind. F_s is most pronounced in areas where the wind is tending to rotate isotherms significantly, i.e., in zones of strong warm and cold advection.

Fig. 16

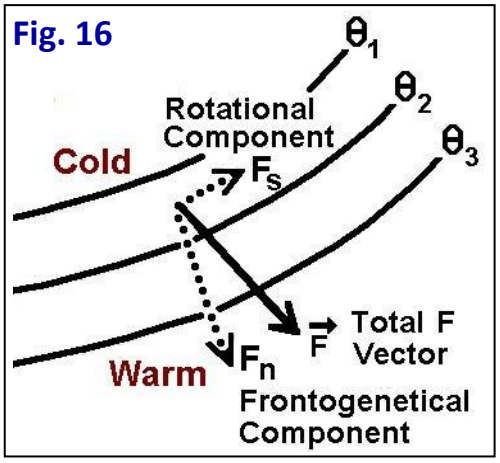

As evident in this case, **the axis or area of QG frontogenesis** (e.g., **Fig. 14B**) **often is broader than Petterssen's 2-D frontogenesis** (e.g., **Fig. 15A**). Similarly, **Q vector convergence zones** (e.g., **Fig. 14C**) **are normally broader than F vector convergence axes** (e.g., **Fig. 15B**). **This makes sense as Q vectors are associated with geostrophic motion and synoptic scale forcing, while F vectors are associated with the total wind and mesoscale forcing. A useful approach in operational forecasting is to overlay F vector forcing in lower-levels (where frontal zones are most pronounced) with Q vector forcing in mid-to-upper levels associated with synoptic flow and shortwaves in the atmosphere.** Coupled with adequate moisture, this method allows the ability to assess mesoscale banded precipitation potential within a field of general precipitation associated with broader scale lift.

Fig. 17 depicts Q vectors associated with an idealized entrance region of a jet streak. Solid lines are height contours, dashed lines are isotherms, and arrows are Q vectors. The thermal gradient increases progressing downwind into the entrance region (from left to right in the figure). The magnitude of Q is largest within the tight thermal gradient and smallest where $\partial T/\partial y$ is weakest. Thus, within the left entrance region of this straight jet streak, there is Q vector divergence forcing descent, while in the right entrance region, Q vector convergence and ascent exist. Ageostrophic winds in this example will be northerly (same direction) below this level (in lower levels) and southerly (opposite direction) above this level (in upper levels). Thus, the Q vectors have defined the thermally direct ageostrophic circulation within the entrance region with ascent in the right entrance area characterized by low-level convergence and upper-level divergence.

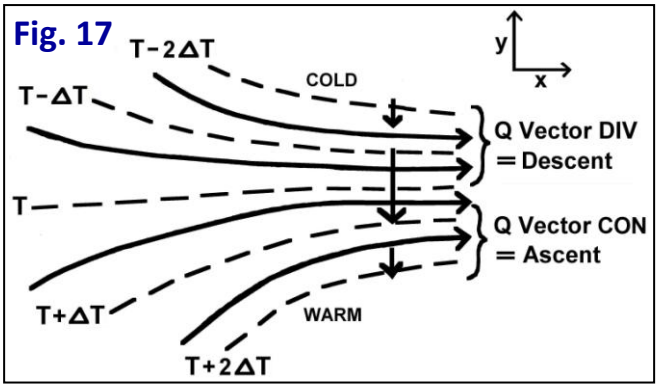

ATMOSPHERIC RESPONSE TO GEOSTROPHIC DEFORMATION

The atmosphere would remain in geostrophic and thermal wind balance, with the thermal field in balance with the height and wind field if straight, frictionless, uniform flow existed at all levels and times. This is not the case. Forcing mechanisms and wind acceleration/deceleration cause disruptions in thermal wind balance, as the geostrophic wind advects the thermal field around. This especially is true for jet streaks. **Within exit (entrance) regions, higher (lower) geostrophic wind speeds are moving into an area** (Point A in **Figs. 18A and 18B**) **where the temperature gradient is too broad (tight) to balance the incoming stronger (lighter) winds. In effect, the geostrophic wind is deforming the thermal field (geostrophic deformation) so that it is out of thermal wind balance. The greater the wind speed changes along the jet, the greater is the deformation. Thus, there must be an atmospheric response in order to restore balance between the thermal and wind fields. This secondary response is achieved through vertical motion (ω) and the ageostrophic wind (v_{ag}), which combine to create a mutual adjustment to increase or decrease the thermal gradient AND increase or decrease the magnitude of the geostrophic wind.**

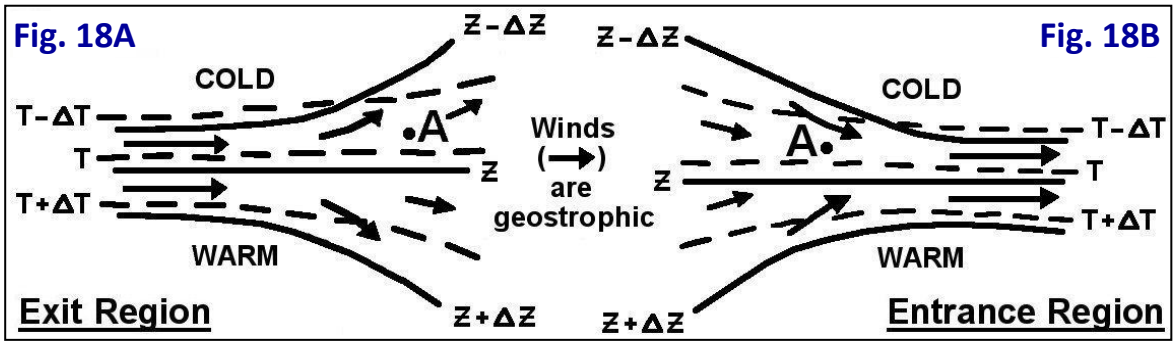

To explore this concept further, consider the jet exit region in **Fig. 18A**. The geostrophic wind (arrows) is decreasing exiting the jet streak core so that kinetic energy is being transformed to available potential energy. At Point A, stronger geostrophic winds are approaching, which will destroy balance as the stronger winds move downstream into the existing weaker thermal gradient at A. As a result, ageostrophic motion and a secondary circulation (vertical motion) must occur to create a mutual

adjustment to regain balance. The atmosphere needs to strengthen the thermal gradient. To do so, cold air must rise and adiabatically cool on the cold side, while warm air must sink and adiabatically warm on the warm side of the jet. This represents the thermally indirect ageostrophic circulation within the exit region of a jet streak. In addition, the Coriolis force acts to increase the low-level westerly momentum, and decrease the upper-level westerly momentum (as northerly ageostrophic flow aloft turns right against the geostrophic flow), which decreases the westerly wind shear with height. The mutual adjustment is now complete, as the atmosphere has tightened the thermal gradient and decreased the westerly geostrophic winds at point A to restore thermal wind balance in the exit region of jet streaks.

In the jet entrance region (**Fig. 18B**), the geostrophic wind is increasing entering the jet core (available potential energy is being transformed to kinetic energy). At Point A, the wind is actually *decreasing* as lower speeds move toward A. The weaker winds now will be out of balance with the existing stronger thermal gradient at A. To restore balance, the thermal gradient must relax and/or the geostrophic winds must increase at A (mutual adjustment). The thermal gradient is weakened through vertical motion, namely the thermally direct circulation of the ageostrophic wind within the entrance region. Warm air rises and cools adiabatically on the warm side of the jet, while cold air sinks and warms adiabatically on the cold side. Balance also is restored as the Coriolis force acts on the ageostrophic winds within the direct circulation. At low-levels, the Coriolis "deflects" northerly ageostrophic winds to the right which opposes and thus decreases westerly low-level momentum. At upper-levels, southerly ageostrophic flow deflected to the right adds to the westerly geostrophic wind, thereby increasing wind speeds at A. This produces an increase in the westerly wind shear with height to help compensate for the tight thermal gradient in the entrance region. The mutual adjustment is now complete. Ageostrophic flow, vertical motion, and the Coriolis force work together to decrease the thermal gradient and increase the westerly momentum in order to restore thermal wind balance within jet entrance regions.

To summarize, **geostrophic forcing inherently destroys thermal wind balance as varying wind fields become out of balance with existing thermal fields. To restore balance, the atmosphere performs a mutual adjustment process through ageostrophic flow and vertical motion. In jet entrance regions, a thermally direct transverse ageostrophic circulation decreases the thermal gradient (to adjust to the approaching weaker winds) and increases the approaching geostrophic flow (to adjust to the existing stronger thermal gradient). In exit regions, a thermally indirect transverse ageostrophic circulation strengthens the thermal gradient (to adjust to the approaching stronger winds) and decreases the approaching geostrophic flow (to adjust to the existing weaker temperature gradient).**

Vertical motion is required within jet exit and entrance regions. The stronger the wind speed gradient (rate of change of the wind) per unit distance along the flow (along-stream variation) and normal to the flow (cross-stream variation), the greater the geostrophic deformation will be, and the greater the restoring vertical motion fields must be to preserve balance.

JET STREAK BASICS AND VERTICAL MOTION PATTERNS

It is apparent **why** vertical motion must occur within jet exit and entrance regions, but **where** the ascent and descent will be located with respect to the jet core is not always clear. In general, jet streaks move slower at roughly one-third the speed of the actual winds blowing through them.

Fig. 19 reveals a model for an idealized, basic straight jet streak. **Fig. 19A** reveals a 4-cell pattern of

convergence/divergence, where arrow length is proportional to the magnitude of ageostrophic flow. The flow is "**subgeostrophic**" (total wind less than geostrophic wind) in the entrance region, and "**supergeostrophic**" in the exit region of the jet. Lines $A - A'$ and $B - B'$ in **Fig. 19A** define the vertical cross-sections shown in **Fig. 19B**. The direct thermal circulation ($A - A'$) occurs in the entrance region; the indirect circulation ($B - B'$) occurs in the exit region. **Fig. 19C** depicts the four-cell pattern of PVA/NVA associated with vorticity maxima and jet streaks.

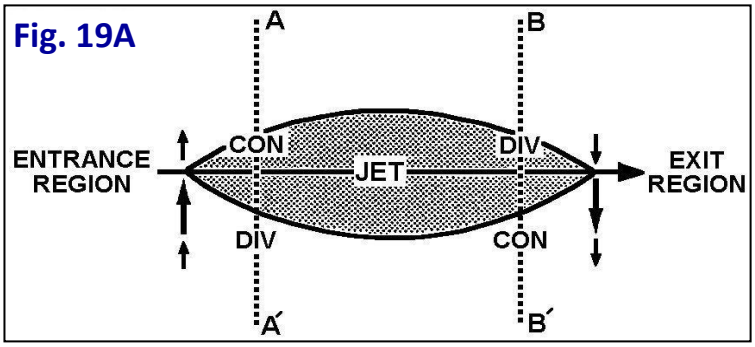

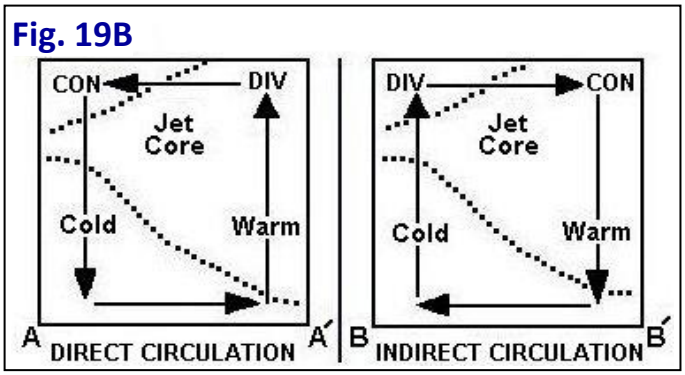

It is known that the "box" circulation in **Fig. 19B** is not what occurs in the atmosphere. The rising and sinking branches of ageostrophic circulations often exhibit a sloped (isentropic) pattern. For example, **Fig. 20** shows a more realistic pattern associated with the exit region of a straight jet streak. Here, the view is looking downstream along the jet core (at "J") so that the exit region is oriented into the page. Divergence (convergence) aloft is occurring within the left (right) exit region (as assumed for straight jets). However, the rising branch of the circulation (bold arrow) is not necessarily vertical on the left exit side. Instead, it is sloped roughly along isentropic (θ) surfaces meaning there could be ascent occurring underneath the jet core or even under the right exit region. The slope could be gradual or quite steep and focused. Depending on stability and the amount of lift and moisture necessary to produce parcel saturation, precipitation could break out not only within the expected left exit region, but also under the jet core or even within the right exit region. This is especially true during the warm season when an unstable air mass needs little forcing to lift parcels to their LFC to form thunderstorms.

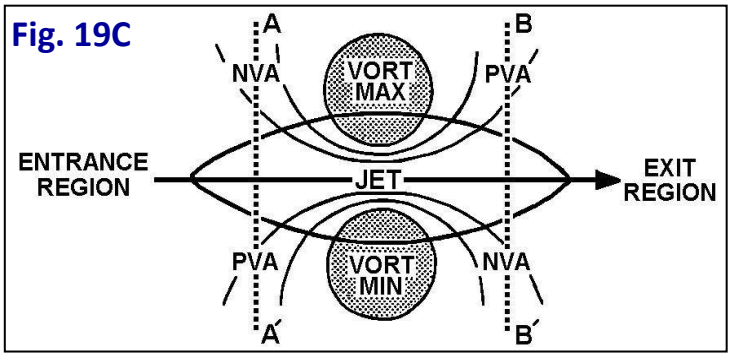

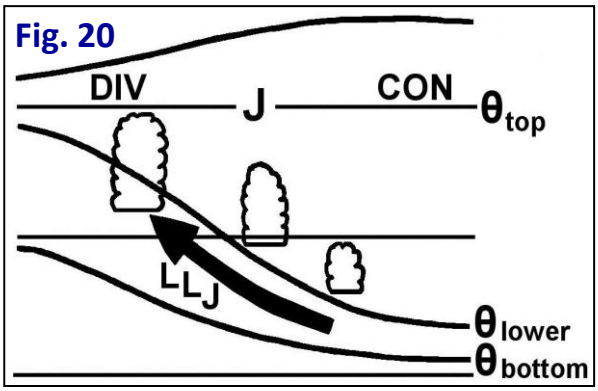

A practical example is provided in **Fig. 21**. The data is from 28 January 2009, when a devastating ice storm over much of Kentucky and southern Indiana was followed by several inches of snow. At 12 UTC, a very pronounced jet streak with some anticyclonic curvature was located from Michigan (150 kt winds) to southern Illinois with appreciable along-stream wind variation in the entrance region, and a strong cross-stream wind gradient on either side of the jet axis (**Fig. 21A**). The 1000-500 mb relative humidity image indicated deep-layer moisture (pink color) over the Ohio Valley. Cutting the cross-section $A - A'$ normal to the jet and thickness field results in the data shown in **Figs. 21B-C**.

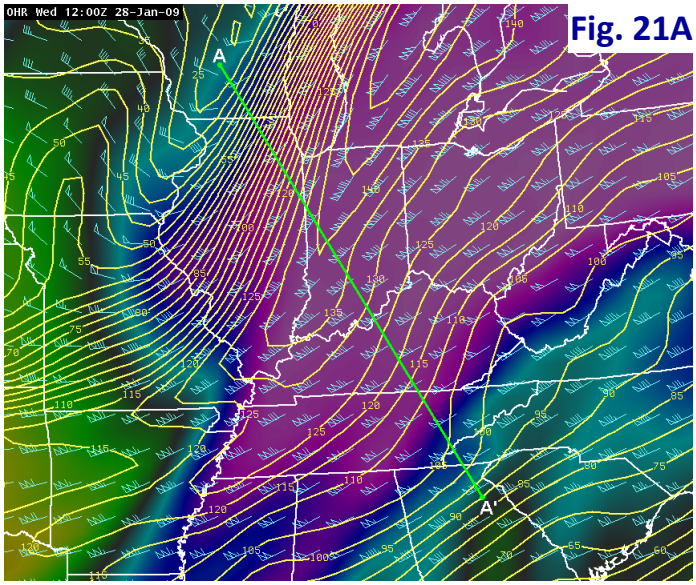

Fig. 21A

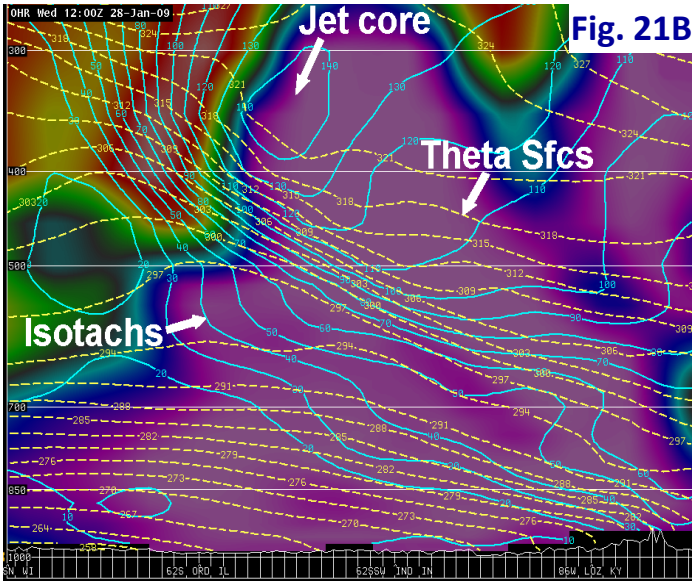

Fig. 21B

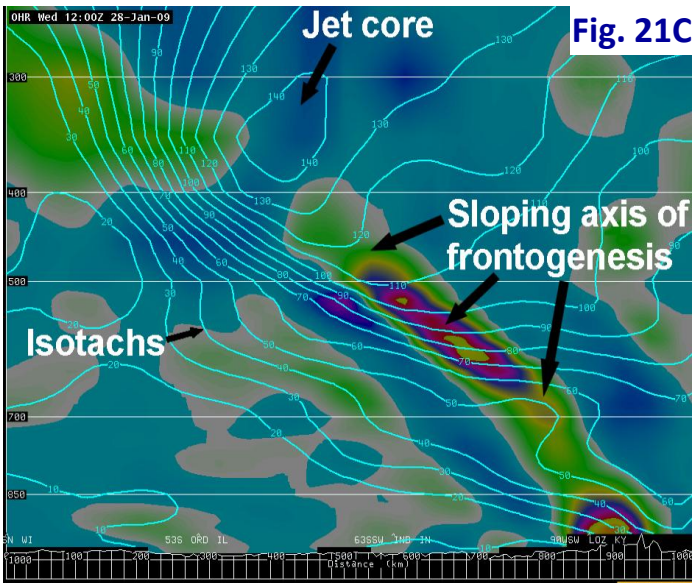

Fig. 21C

The jet core is prominent in **Figs. 21B-C** (blue lines are isotachs) as the cross-sectional plane cuts through west-central Indiana. The area to the right and lower right of the core represents the jet's right entrance region over central Kentucky. The θ surfaces (isentropes; dashed yellow lines) slope upward from southeast- to-northwest toward the upper-level jet core (**Fig. 21B**). This is similar to the idealized graphic shown in **Fig. 20**. Air is rising isentropically along these surfaces. In reality, given moisture, latent heat release, and frontogenetical forcing (**Fig. 21C**), air is likely rising more steeply and flowing off the θ surfaces. Also in **Fig. 21B**, isentropes are tightly packed in the vertical (stable zone) in the center of the image (mid-levels over Kentucky). This represents an elevated frontal zone, along which 2-D frontogenesis is occurring (**Fig. 21C**). The axis of frontogenesis is very deep and sloped with height toward cold air. There are two fronto-genetical maxima, one associated with the surface front in southeastern Tennessee (lower right part of **Fig. 21C**) and the second associated with the mid-level frontal surface which extends up to near the altitude of the jet core. In other words, pronounced frontogenesis is occurring within the right entrance region over Kentucky, where heavy snow was occurring at this time. **The steepness, depth, magnitude, and duration of frontogenetical forcing along with the stability of the atmosphere aloft play integral roles in the development and maintenance of strong vertical motion and formation of heavy banded precipitation. In general, the lower the static stability (less stable), the greater the vertical motion response will be to a given amount of forcing.** It is very interesting to visualize a frontogenetical surface rising toward a jet entrance region within the thermally direct ageostrophic circulation.

As part of the indirect circulation within an exit region (particularly westerly jets), **the southerly low-level ageostrophic branch adds to the existing southerly flow, enhancing the low-level jet**. Increased wind is reflected on pressure and isentropic surfaces, enhancing isentropic lift and precipitation given adequate moisture transport. So, if a low-level jet increases as a jet exit region is approaching, this is no coincidence. **Jet streaks and isentropic analysis are not independent**. Consider the example in **Fig. 22**.

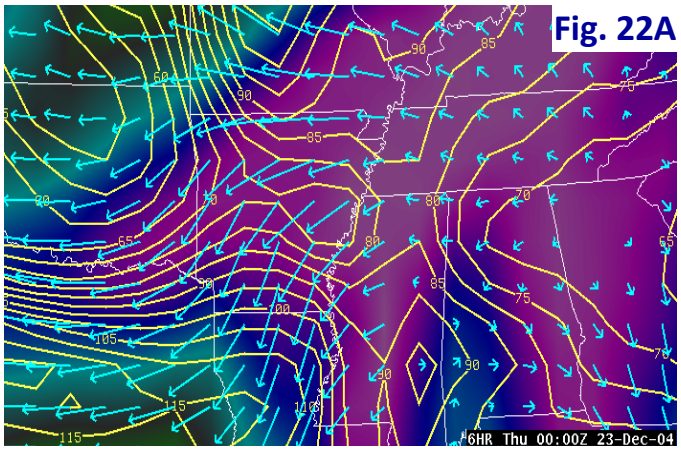

Fig. 22A

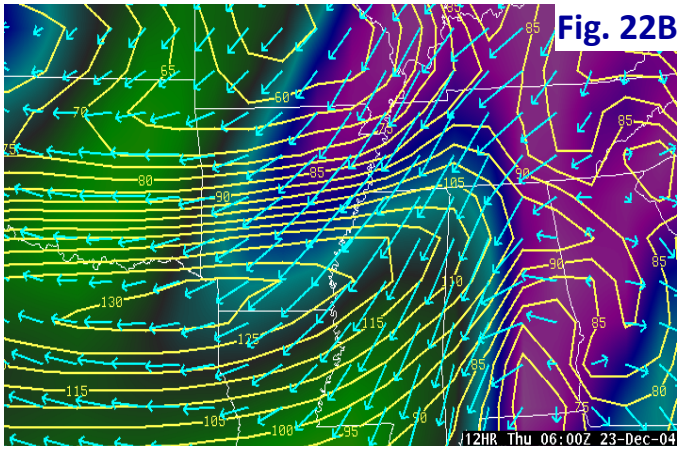

Fig. 22B

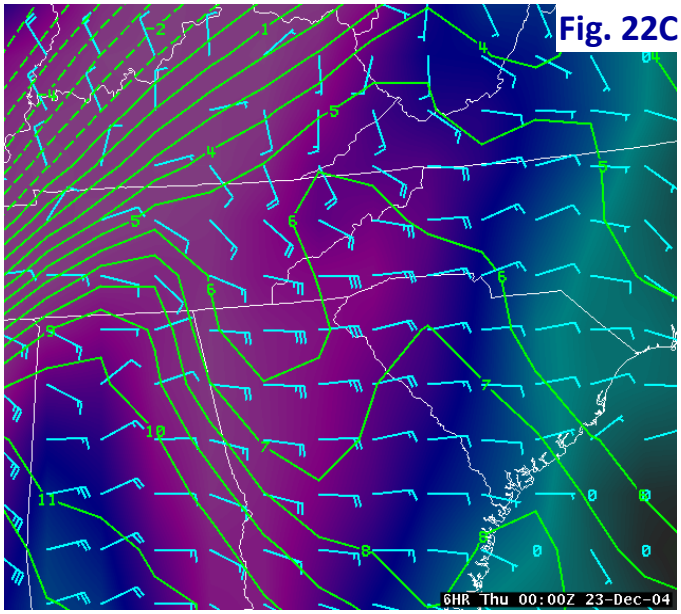

Fig. 22C

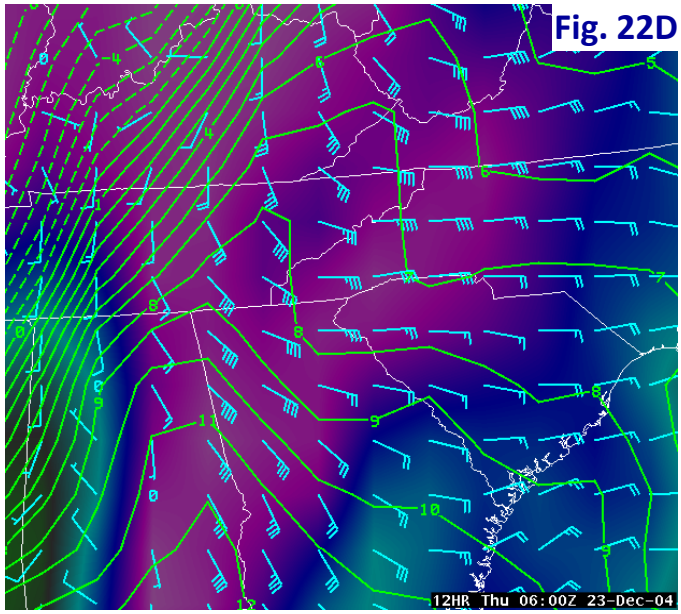

Fig. 22D

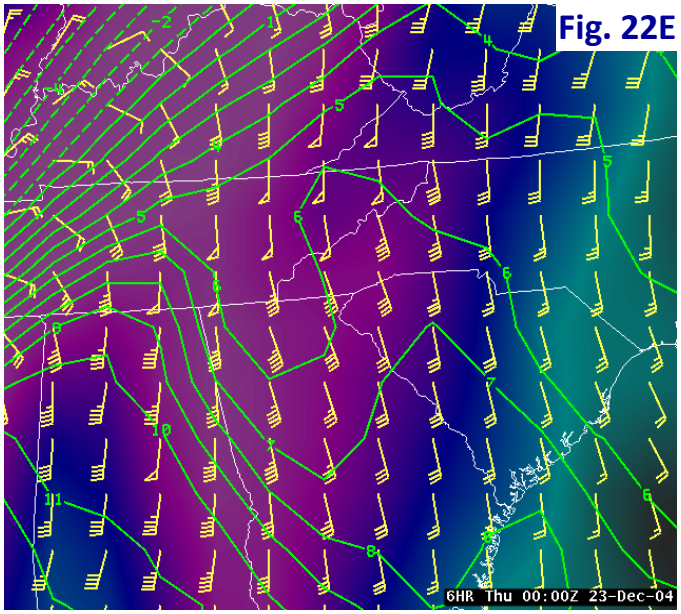

Fig. 22E

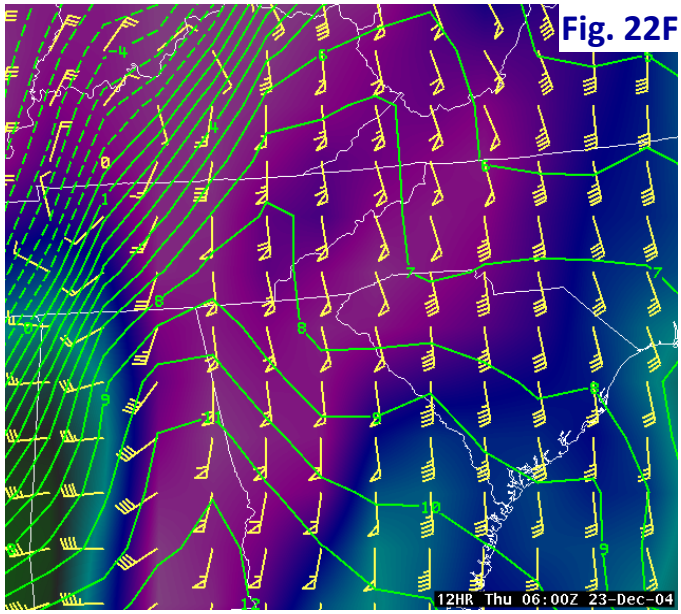

Fig. 22F

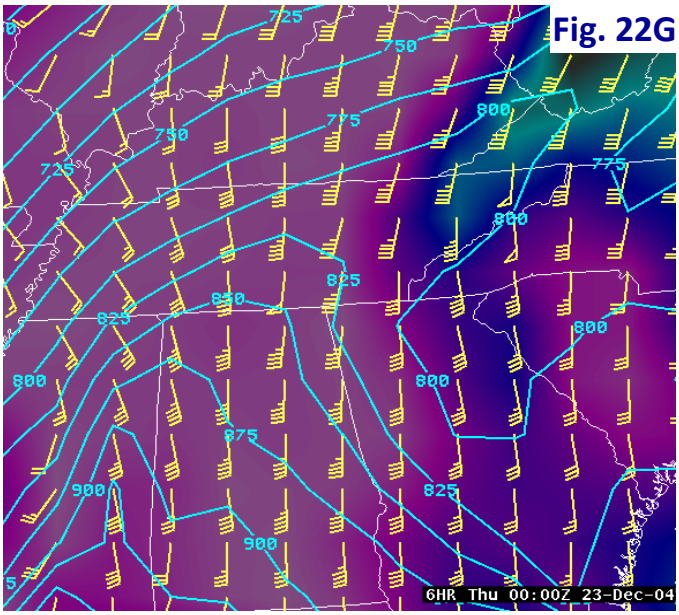

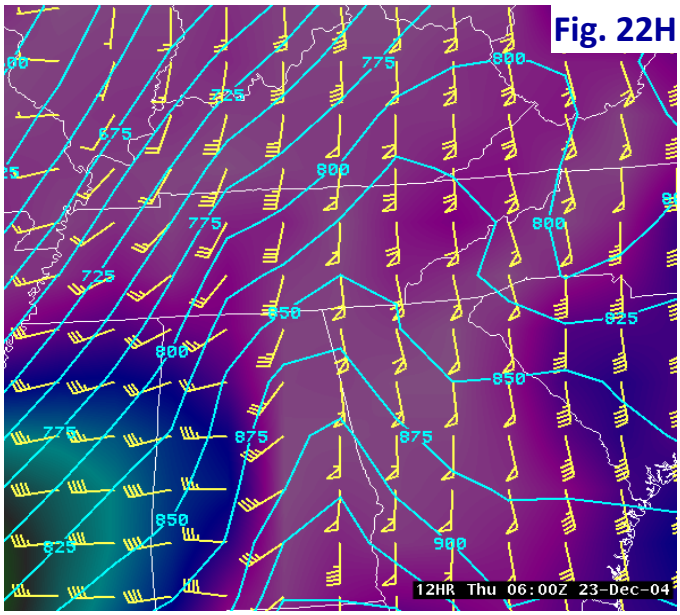

Fig. 22A shows 300 mb isotachs (yellow lines) and ageostrophic winds (blue arrows; speed proportional to length), and 1000-500 mb relative humidity (pink equals near saturation) from the GFS model at 0000 UTC 23 December 2004. A jet core with maximum winds around 120 kts was located over central Texas, with the exit region over the Lower Mississippi Valley/Gulf States. Six hours later (**Fig. 22B**), the jet core was forecast to move east and intensify to around 130 kts. Significant along-stream variation existed in the exit region over the northern Gulf States and Tennessee. Ageostrophic winds at 300 mb implied strong upper-level divergence along and left (poleward) of the exit region. In response, 850 mb ageostrophic winds were forecast to increase and back in direction from eastern Alabama and Georgia to eastern Kentucky between 0000 and 0600 UTC (**Figs. 22C-D**). As a result, the GFS dramatically strengthened the low-level jet (total wind) at 850 mb from 40-50 kts at 0000 UTC (**Fig. 22E**) to 60-70 kts at 0600 UTC (**Fig. 22F**). Correspondingly, an increase in low-level flow and lift was indicated on the 295 K isentropic surface from the Gulf States through Kentucky along the warm conveyer belt (pressure/ thermal ridge axis) (**Figs. 22G-H**). This dynamic interaction and response between the upper-level and low-level jet is very clear in this event, and facilitated strong frontogenetical forcing leading to very heavy snow over southern Indiana to heavy rain and convection in Tennessee southward.

A very important factor which complicates the classic four-cell straight jet streak pattern is curvature. For straight flow, the **cross-stream component of the ageostrophic wind produces patterns of divergence and convergence due to accelerations (entrance regions) and decelerations (exit regions) in the flow** (**Fig. 19A**). On the other hand, the **along-stream component of the ageostrophic wind produces divergence and convergence due to curvature**. Consider **Fig. 23**. Solid lines show the total flow pattern from west to east (left to right). Arrows represent along-stream ageostrophic winds, which point downwind at the top of a ridge axis and upwind in the base of a trough. As a result, **divergence of the ageostrophic wind is produced between the trough and downstream ridge, with convergence between the trough and upstream ridge**. The shorter the wavelength (distance) between the trough and downstream ridge, the greater will be the upper-level divergence.

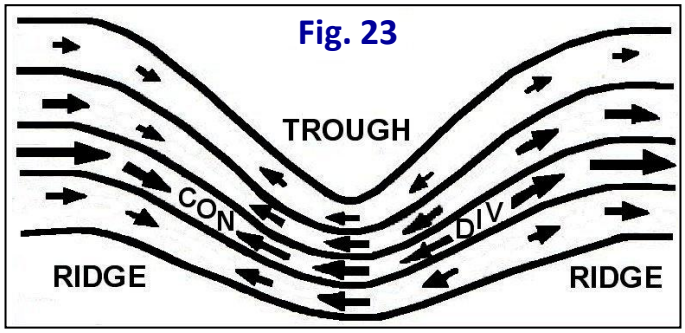

In the base of a trough (top of a ridge), the total wind (v) is sub-geostrophic (supergeostrophic), i.e., the geostrophic wind (v_g) is higher (lower) than the actual wind, so the ageostrophic wind (v_{ag}) direction must be opposite (the same as) that of the geostrophic wind so that $v_g + v_{ag} = v$ (**Fig. 24**). **Divergence (convergence) downstream (upstream) of the trough axis is due to subgeostrophic flow at the base of the trough and supergeostrophic flow at the top of the ridge.**

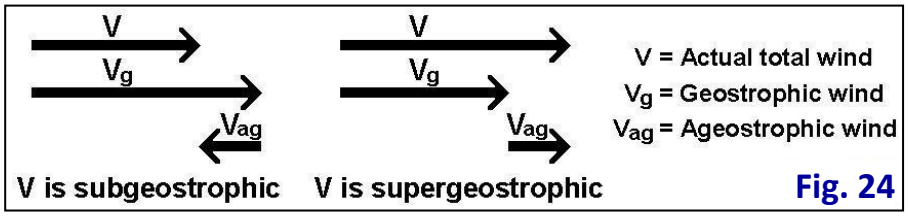

Fig. 24

When a jet streak is embedded within curvature in the flow, both the along-stream and cross-stream components of the ageostrophic wind are important. **Fig. 25** (Moore and VanKnowe 1992) shows the effect of curvature on jet streak vertical motion patterns. The thick line represents the jet core; dashed (solid) lines are areas of ascent (descent) ($10^{-1}\mu b\ s^{-1}$) at 600 mb. **Fig. 25A** reveals the expected basic four-cell pattern for a **straight jet streak: divergence/ascent in the left exit and right entrance regions, and convergence/descent in the right exit and left entrance regions.** With curvature, the four-cell pattern often reduces to two-cells while magnitudes increase. **For a cyclonically-curved jet, the ascent/ descent couplet is aligned near the jet axis, with maximum lift along and left (poleward) of the jet core, but with some ascent also in the right exit region (Fig. 25B). For an anticyclonically-curved jet streak, the greatest ascent is along and right (equatorward) of the core (Fig. 25C).**

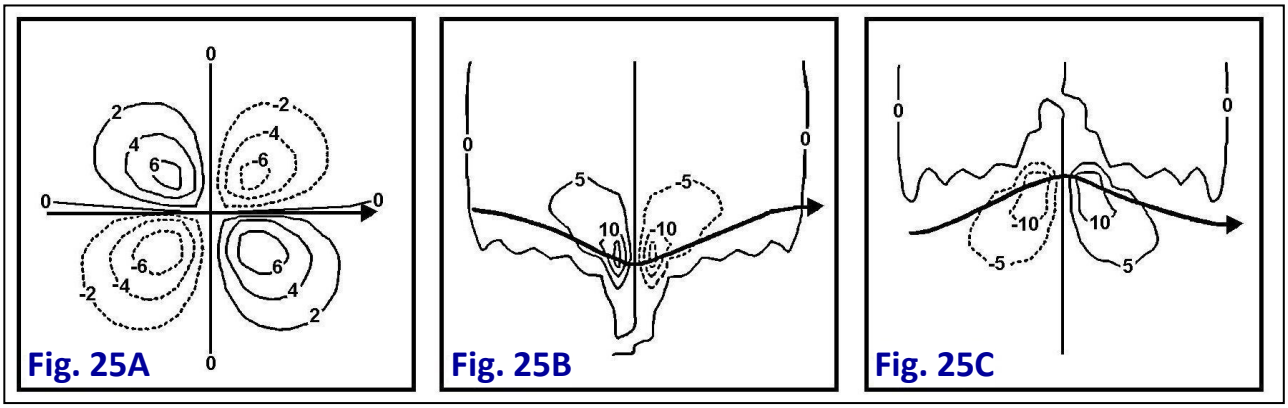

The magnitude of vertical motion is normally greater for curved jets than straight jets as the combined exit-entrance (Fig. 19A), trough-ridge (Fig. 23) system requires more mutual adjustment and, therefore, more vertical motion to restore thermal wind balance in the atmosphere. Overall, vertical motion is strongest for a cyclonically-curved jet streak, then an anticyclonically-curved jet, and weakest but still important for a straight jet. The ascent in a cyclonically-curved exit region results from the combined effect of divergence in the exit region due to the cross-stream ageostrophic wind (Fig. 19A) and divergence between the trough and downstream ridge due to the along-stream ageostrophic wind (Fig. 23). In an anticyclonically-curved entrance region, divergence between the ridge and upstream trough (along-stream component) combines with divergence in the entrance region (cross-stream component).

Another significant factor is the existence and proximity of two jets. A number of studies (e.g., Uccellini and Johnson 1979; Uccellini and Kocin 1990; Hakim and Uccellini 1992) have documented **the importance of jet streak interaction or the merger (coupling) of the ascending branches of two separate jet streaks. The ascent occurs in the rising branch of the thermally direct ageostrophic circulation within the entrance region of one jet, and the thermally indirect circulation within the exit region of the other jet.**

<u>This interaction maximizes upper-level divergence and, therefore, upward motion and precipitation</u>.

Fig. 26 provides an example of jet streak coupling from 23 December 2004 when up to 30 inches of snow fell over parts of south-central Indiana, with heavy snow, sleet, and rain over central Kentucky. At 0600 UTC, an anticyclonically-curved jet streak was located from Illinois to the western Great Lakes, while a cyclonically-curved jet was oriented from Texas to Tennessee (**Fig. 26A**). The right entrance region of the northern jet and left exit region of the southern jet were juxtapositioned over the Lower Ohio Valley. Total ageostrophic winds (along- and cross-stream components) at 300 mb (blue arrows) implied strong upper-level divergence over this area in the favored quadrants of both jet streaks.

Fig. 26B shows a spatial-height cross-section at 0600 UTC along line $A - A'$ from northwest Wisconsin to central Georgia (**Fig. 26A**). Similar to **Fig. 21C**, a deep-layered axis of frontogenesis (green, yellow, and white colors in image) was sloped with height toward cold air from the surface front/boundary layer in southeastern Tennessee (lower right part of figure) all the way to the core of the northern jet streak over southern Wisconsin. The frontogenesis was within the right entrance region of the jet, as is common in baroclinic systems. Above the axis of frontogenesis was an area of reduced atmospheric stability, as indicated by negative values of saturated equivalent potential vorticity (EPV; dashed blue lines). Negative

Fig. 26A

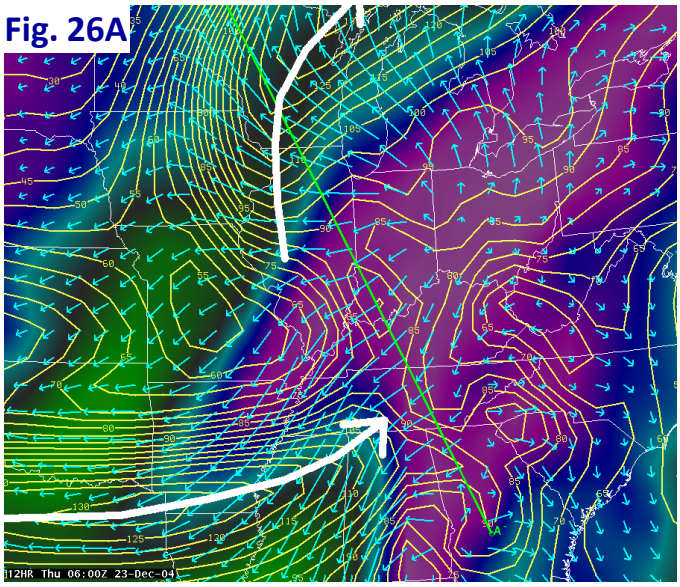

Fig. 26B

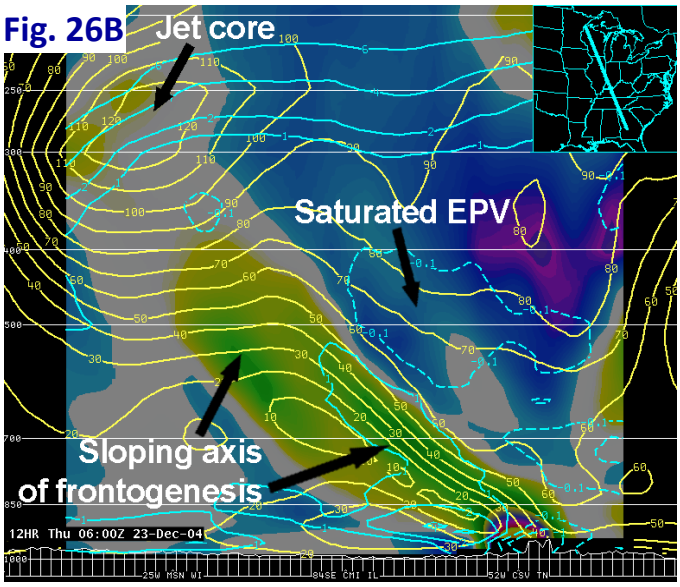

EPV values suggest the atmosphere is potentially unstable to moist slantwise or vertical accelerations (Moore and Lambert 1993), and can result in greater vertical velocities for a given amount of forcing than in a stable or laminar atmosphere. In addition, the number and intensity (reflectivity) of resulting precipitation bands can increase with diminishing stability/increasing instability in the atmosphere (**Fig. 27**). This can change precipitation from more stratiform in nature to more convective (whether or not thunder and lightning occurs). In this event, the substantial frontogenetical forcing combined with lessened stability aloft (**Fig. 26B**) was an excellent set up for intense vertical motion

Fig. 26C

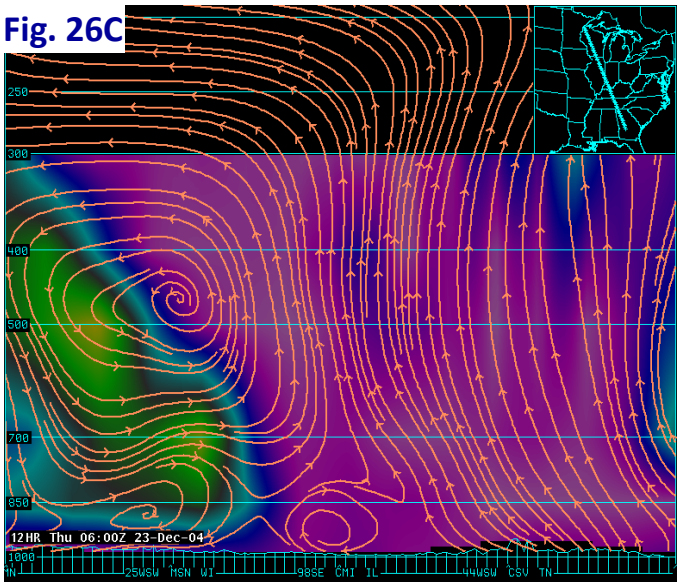

and very heavy banded snowfall. In fact, thunder and lightning was observed during the period of highest precipitation rates.

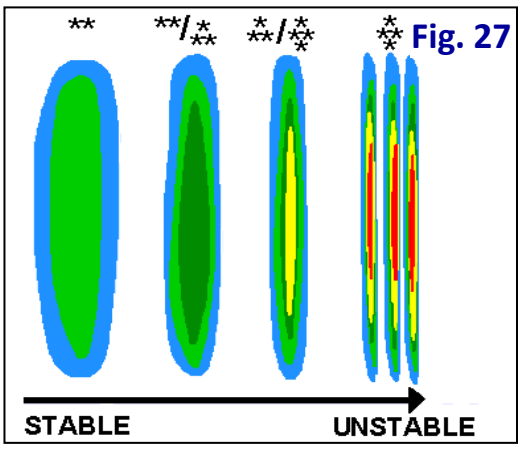

Additional reading on the role of EPV and frontogenetical forcing in producing significant banded precipitation in extra-tropical storms can be found in Nicosia and Grumm (1999), and Wiesmueller and Zubrick (1998), among others.

Fig. 26C represents the vertical circulation of the ageostrophic wind. The thermally direct circulation in the entrance region is very apparent. Deep, strong ascent associated with frontogenetical forcing is noted within the area of saturation (pink color in relative humidity image; truncated at 300 mb), particularly from about 700-300 mb over the Lower Ohio Valley (center portion of **Fig. 26C**). At high altitudes, horizontal southeast-to-northwest flow is evident (upper left part of **Fig. 26C**), representing the cross-component of the ageostrophic wind traversing the jet from the right entrance to left entrance region. Within the circulation, downward motion is noted to the left of the jet core, i.e., the far left side of **Fig. 26C**. To complete the circulation, quasi-horizontal northwest-to-southeast oriented ageostrophic motion is present in lower-levels (centered roughly from 800-650 mb) over the northwest section of the cross-section under the jet core (lower left part of **Fig. 26C**), helping import or keep cold air in place over the Ohio Valley. As expected, the upward components of the circulation are strongest and the most concentrated. The thermally indirect circulation associated with the exit region of the southern jet in **Fig. 26A** is less evident, but suggested via ascent in the southern portion of the cross-section (right part of **Fig. 26C**). Part of this circulation may also be out of the plane of the $A - A'$ cross-sectional line.

The thermally direct ageostrophic circulation in **Fig. 26C** replicates the idealized circulation depicted by Carlson 1998 (**Fig. 28A**) and Emanuel 1985 (**Fig. 28B**). The rising component is in the relatively warmer air and sloped toward colder air with height, with descent in the colder (poleward) air. The horizontal components cross the jet ("*J*") at high altitudes with divergence aloft within the right entrance region. **Fig. 28B** also shows that the ascending branch typically is stronger and more concentrated (given the presence of low static stability) than the broader, weaker descending branch. This relates well to that seen in the 23 December 2004 case, where a dual jet structure, pronounced frontogenetical forcing, and low stability aloft (negative values of EPV) resulted in very strong ascent (**Figs. 26A-C**).

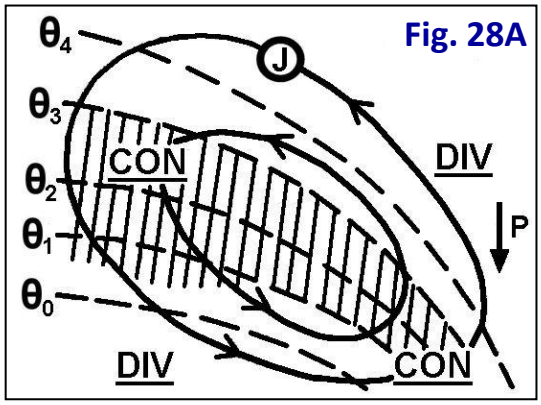

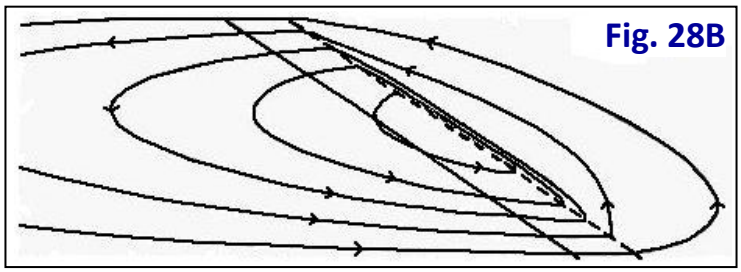

To summarize, it is important to differentiate the geostrophic and ageostrophic components of the total wind because **1) QG theory is based on the geostrophic wind and used to explain physical atmospheric processes, 2) departure from geostrophy causes significant weather, so analysis of the**

geostrophic and ageostrophic wind is essential, 3) it is the ageostrophic wind which is divergent/ convergent and leads to vertical motion, and 4) the ageostrophic wind and vertical motion response are the mechanisms by which geostrophic/thermal wind balance is restored in the atmosphere.

DOCUMENT SUMMARY

This document is intended to serve as an easy reference of basic background information on quasi-geostrophic theory and related physical mechanisms and processes. A much more thorough knowledge of synoptic and dynamic meteorology can be found in such textbooks as Bluestein (1992, 1993), Haltiner and Williams (1980), Holton (1979), and others. Such knowledge is essential to accurate weather prediction. While this document is far from a technical, all-inclusive explanation of the discussed processes, it attempts to answer "why" and "how" processes work the way they do in the atmosphere in basic terms. It also provides a sound basis from which to draw upon in evaluating synoptic and some mesoscale situations within the scientific reasoning and forecast preparation process.

REFERENCES

Bluestein, H.B., 1992: *Synoptic-Dynamic Meteorology in Midlatitudes, Volume I – Principles of Kinematics and Dynamics*. New York: Oxford University Press.

Bluestein, H.B., 1993: *Synoptic-Dynamic Meteorology in Midlatitudes, Volume II – Observations and Theory of Weather Systems*. New York: Oxford University Press.

Carlson, T.N., 1998: *Mid-Latitude Weather Systems*. Boston: American Meteorological Society.

Emanuel, K.A., 1985: Frontal circulations in the presence of small moist symmetric stability. *J. Atmos. Sci.*, **42**, 1062-1071.

Hakim, G.J., and L.W. Uccellini, 1992: Diagnosing coupled jet streak circulations for a Northern Plains snow band from the operational Nested-Grid Model. *Wea. Forecasting*, **7**, 26-48.

Haltiner, G.J., and R.T. Williams, 1980: *Numerical Prediction and Dynamic Meteorology*. New York: Wiley.

Holton, J.R., 1979: *An Introduction to Dynamic Meteorology*. Orlando: Academic Press.

Hoskins, B.J., and M.A. Peddler, 1980: The diagnosis of middle latitude synoptic development. *Quart. J. Roy. Meteor. Soc.*, **106**, 707-719.

Hoskins, B.J., I. Draghici, and H.C. Davies, 1978: A new look at the ω-equation. *Quart. J. Roy. Meteor. Soc.*, **104**, 31-38.

Moore, J.T., and G.E. VanKnowe, 1992: The effect of jet-streak curvature on kinematic fields. *Mon. Wea. Rev.*, **120**, 2429-2441.

Moore, J.T., and T.E. Lambert, 1993: The use of equivalent potential vorticity to diagnose regions of

conditional symmetric instability, *Wea. Forecasting*, **8**, 301-308.

Nicosia, D. J., and R. H. Grumm, 1999: Mesoscale band formation in three major northeastern United States snowstorms. *Wea. Forecasting.* **14,** 346-368.

Petterssen, S., 1956: Motion and Motion Systems. Vol. I. Weather Analysis and Forecasting. New York: McGraw Hill.

Trenberth, K.E., 1978: On the interpretation of the diagnostic quasi-geostrophic omega equation. *Mon. Wea. Rev.*, **106**, 131-137.

Uccellini, L.W., and D.R. Johnson, 1979: The coupling of upper and lower tropospheric jet streaks and implications for the development of severe convective storms. *Mon. Wea. Rev.*, **107**, 682-703.

Uccellini, L.W., and P.J. Kocin, 1990: The interaction of jet streak circulations during heavy snow events along the east coast of the United States. *Wea. Forecasting*, **2**, 298-308.

Wiesmueller, J. L., and S. M. Zubrick, 1998: Evaluation and application of conditional symmetric instability, equivalent potential vorticity, and frontogenetical forcing in an operational forecasting environment. *Wea. Forecasting,* **13,** 84-101.